

JAERI - M
84-071

X-RAY PHOTOELECTRON AND X-RAY-INDUCED
AUGER ELECTRON SPECTROSCOPIC DATA, II
-4d TRANSITION-METALS (Y, Zr, Nb, Mo, Ru)
AND RELATED OXIDES -

April 1984

Yuji BABA and Teikichi A. SASAKI

日本原子力研究所
Japan Atomic Energy Research Institute

JAERI-Mレポートは、日本原子力研究所が不定期に公刊している研究報告書です。
入手の問い合わせは、日本原子力研究所技術情報部情報資料課（〒319-11茨城県那珂郡東海村）あて、お申しこしください。なお、このほかに財団法人原子力弘済会資料センター（〒319-11茨城県那珂郡東海村日本原子力研究所内）で複写による実費頒布をおこなっております。

JAERI-M reports are issued irregularly.
Inquiries about availability of the reports should be addressed to Information Section, Division of Technical Information, Japan Atomic Energy Research Institute, Tokai-mura, Naka-gun, Ibaraki-ken 319-11, Japan.

©Japan Atomic Energy Research Institute, 1984

編集兼発行 日本原子力研究所
印刷 榎高野高速印刷

X-RAY PHOTOELECTRON AND X-RAY-INDUCED AUGER ELECTRON SPECTROSCOPIC DATA, II
— 4d TRANSITION-METALS (Y, Zr, Nb, Mo, Ru) AND RELATED OXIDES —

Yuji BABA and Teikichi A. SASAKI

Department of Chemistry, Tokai Research Establishment, JAERI

(Received March 8, 1984)

The intrinsic data of the X-ray photoelectron spectra (XPS) and X-ray-induced Auger electron spectra (XAES) for 4d transition-metals and related oxides were obtained by means of a spherical electron spectrometer. The metallic surfaces were cleaned by two different methods : mechanical filing and Ar⁺ ion etching. In the case of the Ar⁺ ion bombarded Y, Zr, and Nb metals, the binding energies of the core-lines and the kinetic energies of the Auger lines shift from those for the mechanically filed surfaces. The energy shifts were interpreted in terms of the ion-induced lattice distortion of the metal surfaces. The oxides examined are typical compounds such as Y₂O₃, ZrO₂, Nb₂O₅, MoO₃ and RuO₂. The data consists of 4 wide scans, 33 core-line spectra, 10 valence-band spectra and 12 XAES spectra. The peak positions of the core-lines and the Auger lines were summarized in 6 tables together with their chemical shifts.

KEYWORDS :

X-ray Photoelectron Spectroscopy, X-ray-induced Auger Electron Spectroscopy, Yttrium, Zirconium, Niobium, Molybdenum, Ruthenium, Y₂O₃, ZrO₂, Nb₂O₅, MoO₃, RuO₂, Sputtering

This work was done by the use of an ESCA spectrometer connected with the JAERI Tandem Accelerator.

X線光電子及びX線励起オージェ電子スペクトルデータ II
—4d遷移金属 (Y, Zr, Nb, Mo, Ru) 及びその酸化物—

日本原子力研究所東海研究所原子炉化学部

馬場 祐治・佐々木 貞吉

(1984年3月8日受理)

4d遷移金属とその酸化物について、半球型電子エネルギー分析器によりX線光電子分光スペクトル (XPS) 及びX線励起オージェ電子スペクトル (XAES) を測定した。金属の真正表面は、2通りの異なる方法、すなわち超高真空中やすり研摩法及びアルゴンイオンエッチング法で得た。アルゴンイオン照射した金属試料では、内殻電子の結合エネルギー及びオージェ電子の運動エネルギーは、やすり研摩した場合と異なった値を示す。このエネルギーシフトは、イオン照射で誘起された結晶格子の表面損傷によると考えられる。また、 Y_2O_3 , ZrO_2 , Nb_2O_5 , MoO_3 , RuO_2 などの酸化物についても測定を行った。本報は4種のワイドスキャン、33種の内殻スペクトル、10種の価電子帯スペクトル及び12種のXAESスペクトルから成る。内殻電子の結合エネルギー、オージェ電子の運動エネルギー及びオージェパラメーターは、化学シフトと共に表にまとめた。

CONTENTS

1. Introduction	1
2. Preparation of samples	1
3. Spectral measurements	2
4. Data interpretation	2
4. 1 General description	2
4. 2 Metal surfaces	2
4. 3 Oxides	4
REFERENCES	6

目 次

1. 序	1
2. 試料調製	1
3. スペクトル測定法	2
4. データの説明	2
4.1 概説	2
4.2 金属表面	2
4.3 酸化物	4
参考文献	6

LIST OF TABLES

- Table 1 Binding energies and chemical shifts of the core-lines for Y_{fl}^* , Y_{et}^{**} and Y_2O_3 .
- Table 2 Binding energies and chemical shifts of the core-lines for Zr_{fl} , Zr_{et} and ZrO_2 .
- Table 3 Binding energies and chemical shifts of the core-lines for Nb_{fl} , Nb_{et} and Nb_2O_5 .
- Table 4 Binding energies and chemical shifts of the core-lines for Mo_{fl} , Mo_{et} and MoO_3 .
- Table 5 Binding energies of the core-lines for RuO_2 .
- Table 6 Kinetic energies and chemical shifts of the $M_{4,5}N_{2,3}V$ Auger lines for Y, Zr, Nb, Mo and their compounds.
- Table 7 Auger parameters and their shifts from metallic states for Y, Zr, Nb, Mo and their oxides.

* Notation *fl* indicates a mechanical filing.

** Notation *et* indicates an Ar^+ ion etching.

LIST OF FIGURES

- Fig. 1 Binding energy shifts of Nb3d_{5/2} line for Ar⁺ ion bombarded Nb metal as a function of ion fluence.
- Fig. 2 XPS wide scan of Y_{fl}.
- Fig. 3 Y3s XPS spectrum of Y_{fl}.
- Fig. 4 Y3p XPS spectrum of Y_{fl}.
- Fig. 5 Y3d XPS spectrum of Y_{fl}.
- Fig. 6 Y4p XPS spectrum of Y_{fl}.
- Fig. 7 Valence-band spectrum of Y_{fl}.
- Fig. 8 M_{4,5}N_{2,3}^V XAES spectrum of Y_{fl}.
- Fig. 9 Y3d XPS spectrum of Y_{et}.
- Fig. 10 M_{4,5}N_{2,3}^V XAES spectrum of Y_{et}.
- Fig. 11 Y3s XPS spectrum of Y₂O₃.
- Fig. 12 Y3p XPS spectrum of Y₂O₃.
- Fig. 13 Y3d XPS spectrum of Y₂O₃.
- Fig. 14 Valence-band spectrum of Y₂O₃.
- Fig. 15 M_{4,5}N_{2,3}^V XAES spectrum of Y₂O₃.
- Fig. 16 XPS wide scan of Zr_{fl}.
- Fig. 17 Zr3s XPS spectrum of Zr_{fl}.
- Fig. 18 Zr3p XPS spectrum of Zr_{fl}.
- Fig. 19 Zr3d XPS spectrum of Zr_{fl}.
- Fig. 20 Zr4p XPS spectrum of Zr_{fl}.
- Fig. 21 Valence-band spectrum of Zr_{fl}.
- Fig. 22 M_{4,5}N_{2,3}^V XAES spectrum of Zr_{fl}.
- Fig. 23 Zr3d XPS spectrum of Zr_{et}.
- Fig. 24 M_{4,5}N_{2,3}^V XAES spectrum of Zr_{et}.
- Fig. 25 Zr3d XPS spectrum of ZrO₂.
- Fig. 26 Valence-band spectrum of ZrO₂.
- Fig. 27 M_{4,5}N_{2,3}^V XAES spectrum of ZrO₂.
- Fig. 28 XPS wide scan of Nb_{fl}.
- Fig. 29 Nb3s XPS spectrum of Nb_{fl}.
- Fig. 30 Nb3p XPS spectrum of Nb_{fl}.
- Fig. 31 Nb3d XPS spectrum of Nb_{fl}.
- Fig. 32 Nb4p XPS spectrum of Nb_{fl}.

- Fig. 33 Valence-band spectrum of Nb_{fl}.
- Fig. 34 M_{4,5}N_{2,3}V XAES spectrum of Nb_{fl}.
- Fig. 35 Nb3p XPS spectrum of Nb_{et}.
- Fig. 36 Nb3d XPS spectrum of Nb_{et}.
- Fig. 37 Valence-band spectrum of Nb_{et}.
- Fig. 38 M_{4,5}N_{2,3}V XAES spectrum of Nb_{et}.
- Fig. 39 Nb3d XPS spectrum of Nb₂O₅.
- Fig. 40 Valence-band spectrum of Nb₂O₅.
- Fig. 41 M_{4,5}N_{2,3}V XAES spectrum of Nb₂O₅.
- Fig. 42 XPS wide scan of Mo_{fl}.
- Fig. 43 Mo3s XPS spectrum of Mo_{fl}.
- Fig. 44 Mo3p XPS spectrum of Mo_{fl}.
- Fig. 45 Mo3d XPS spectrum of Mo_{fl}.
- Fig. 46 Mo4s XPS spectrum of Mo_{fl}.
- Fig. 47 Mo4p XPS spectrum of Mo_{fl}.
- Fig. 48 Valence-band spectrum of Mo_{fl}.
- Fig. 49 M_{4,5}N_{2,3}V XAES spectrum of Mo_{fl}.
- Fig. 50 Mo3d XPS spectrum of Mo_{et}.
- Fig. 51 M_{4,5}N_{2,3}V XAES spectrum of Mo_{et}.
- Fig. 52 Mo3s XPS spectrum of MoO₃.
- Fig. 53 Mo3p XPS spectrum of MoO₃.
- Fig. 54 Mo3d XPS spectrum of MoO₃.
- Fig. 55 Mo4p XPS spectrum of MoO₃.
- Fig. 56 Valence-band spectrum of MoO₃.
- Fig. 57 M_{4,5}N_{2,3}V XAES spectrum of MoO₃.
- Fig. 58 Ru3p XPS spectrum of RuO₂.
- Fig. 59 Ru3d XPS spectrum of RuO₂.
- Fig. 60 Valence-band spectrum of RuO₂.

1. Introduction

This report presents the intrinsic data of the X-ray photoelectron spectroscopy (XPS) and X-ray-induced Auger electron spectroscopy (XAES) for some 4d transition-metals and their typical oxides. The objects of this report are essentially the same as those described in our previous work dealing with 3d transition-metals.¹⁾

Briefly, the first is to present the XPS spectra which have not been compiled in handbook,²⁾ such as valence-band spectra and core-line spectra with relatively weak intensities. The second is to display the intrinsic XAES spectra, since there has been no available data for the XAES analysis. The third, which is especially emphasized in this report, is to elucidate the spectral difference between metal surfaces etched with Ar⁺ ions and those obtained by mechanical filing. The observed differences were interpreted in terms of the lattice distortion of the metal surfaces.

2. Preparation of samples

Starting materials used were 99.9 % metallic foils. The clean surfaces of the metals were obtained by two different methods. One is a mechanical filing in a preparation chamber under the pressure of 1.3×10^{-8} Pa, and another is an Ar⁺ ion etching. The latter was done by bombarding the mechanically filed metals with 8 keV Ar⁺ ions at a current density of $10 \mu\text{A}/\text{cm}^2$. Figure 1 shows the energy shifts of the Nb $3d_{5/2}$ line for the Ar⁺ ion bombarded Nb metal as a function of the ion fluence. The separation energy is almost proportional to the ion fluence upto $\sim 2 \times 10^{16}$ ions/cm², whereas it saturates at the fluence over $\sim 6 \times 10^{16}$ ions/cm². On the basis of this observation, the Ar⁺ ion bombardment for the compiled data was carried out at the total fluence upto $\sim 10^{17}$ ions/cm².

The oxides such as Y₂O₃, ZrO₂, Nb₂O₅, and MoO₃ were prepared by oxidizing the metallic foils at 300-400°C in an oxygen atmosphere, and RuO₂ was obtained by ignizing metallic powder at 900°C in oxygen atmosphere. Before the spectral measurements, the samples were heated upto 200°C in the spectrometer chamber under the pressure of $\sim 1.3 \times 10^{-7}$ Pa.

1. Introduction

This report presents the intrinsic data of the X-ray photoelectron spectroscopy (XPS) and X-ray-induced Auger electron spectroscopy (XAES) for some 4d transition-metals and their typical oxides. The objects of this report are essentially the same as those described in our previous work dealing with 3d transition-metals.¹⁾

Briefly, the first is to present the XPS spectra which have not been compiled in handbook,²⁾ such as valence-band spectra and core-line spectra with relatively weak intensities. The second is to display the intrinsic XAES spectra, since there has been no available data for the XAES analysis. The third, which is especially emphasized in this report, is to elucidate the spectral difference between metal surfaces etched with Ar⁺ ions and those obtained by mechanical filing. The observed differences were interpreted in terms of the lattice distortion of the metal surfaces.

2. Preparation of samples

Starting materials used were 99.9 % metallic foils. The clean surfaces of the metals were obtained by two different methods. One is a mechanical filing in a preparation chamber under the pressure of 1.3×10^{-8} Pa, and another is an Ar⁺ ion etching. The latter was done by bombarding the mechanically filed metals with 8 keV Ar⁺ ions at a current density of $10 \mu\text{A}/\text{cm}^2$. Figure 1 shows the energy shifts of the Nb_{3d_{5/2}} line for the Ar⁺ ion bombarded Nb metal as a function of the ion fluence. The separation energy is almost proportional to the ion fluence upto $\sim 2 \times 10^{16}$ ions/cm², whereas it saturates at the fluence over $\sim 6 \times 10^{16}$ ions/cm². On the basis of this observation, the Ar⁺ ion bombardment for the compiled data was carried out at the total fluence upto $\sim 10^{17}$ ions/cm².

The oxides such as Y₂O₃, ZrO₂, Nb₂O₅, and MoO₃ were prepared by oxidizing the metallic foils at 300-400°C in an oxygen atmosphere, and RuO₂ was obtained by ignizing metallic powder at 900°C in oxygen atmosphere. Before the spectral measurements, the samples were heated upto 200°C in the spectrometer chamber under the pressure of $\sim 1.3 \times 10^{-7}$ Pa.

3. Spectral measurements

The XPS and XAES measurements were carried out by means of a V.G. ESCALAB-5 spectrometer equipped with a spherical electron analyzer. The base pressure during the measurements was less than 1.3×10^{-8} Pa. A Mg K α X-ray source (1253.6 eV) was operated at 125 W. The spectrometer was calibrated such that the Au4f $_{7/2}$ line appears at $E_b = 84.0$ eV. The FWHM (full-width at half maximum) of the Au4f $_{7/2}$ line was 0.9 eV, and the reproducibility of the spectrometer was within ± 0.1 eV. In the case of the insulating oxides, the original spectra shifted to the higher binding-energy side because of the charging effect. Therefore, the energy scale was aligned to make the peak positions of the metal 3d $_{3/2}$ lines for the oxides and for the most oxidized species on the oxygen-adsorbed metallic surfaces coincide.

4. Data interpretation

4.1 General description

In the tables and figures, the notations *fl* and *et* indicate the procedures of the mechanical filing and Ar⁺ ion etching, respectively. The XPS and XAES spectra for Y_{*fl*}, Y_{*et*} and Y₂O₃ are presented in Figs. 2-15, for Zr_{*fl*}, Zr_{*et*} and ZrO₂ in Figs. 16-27, for Nb_{*fl*}, Nb_{*et*} and Nb₂O₅ in Figs. 28-41, for Mo_{*fl*}, Mo_{*et*} and MoO₃ in Figs. 42-57, and for RuO₂ in Figs. 58-60, respectively. In these figures, the peak position is indicated in eV. The binding energies of the core-lines are summarized in Tables 1-5 and the kinetic energies of the Auger lines are listed in Table 6.

4.2 Metal surfaces

The binding energies of the core-lines for Y_{*et*}, Zr_{*et*}, and Nb_{*et*} shifted to the higher binding energy side by 0.1-1.0 eV from those for the corresponding metallic surfaces obtained by mechanical filing. These core-line shifts have been observed in such metals as Pd,³⁾ Ti,¹⁾ and V.¹⁾

3. Spectral measurements

The XPS and XAES measurements were carried out by means of a V.G. ESCALAB-5 spectrometer equipped with a spherical electron analyzer. The base pressure during the measurements was less than 1.3×10^{-8} Pa. A Mg K α X-ray source (1253.6 eV) was operated at 125 W. The spectrometer was calibrated such that the Au4f $_{7/2}$ line appears at $E_p = 84.0$ eV. The FWHM (full-width at half maximum) of the Au4f $_{7/2}$ line was 0.9 eV, and the reproducibility of the spectrometer was within ± 0.1 eV. In the case of the insulating oxides, the original spectra shifted to the higher binding-energy side because of the charging effect. Therefore, the energy scale was aligned to make the peak positions of the metal 3d $_{3/2}$ lines for the oxides and for the most oxidized species on the oxygen-adsorbed metallic surfaces coincide.

4. Data interpretation

4.1 General description

In the tables and figures, the notations *fl* and *et* indicate the procedures of the mechanical filing and Ar⁺ ion etching, respectively. The XPS and XAES spectra for Y_{*fl*}, Y_{*et*} and Y₂O₃ are presented in Figs. 2-15, for Zr_{*fl*}, Zr_{*et*} and ZrO₂ in Figs. 16-27, for Nb_{*fl*}, Nb_{*et*} and Nb₂O₅ in Figs. 28-41, for Mo_{*fl*}, Mo_{*et*} and MoO₃ in Figs. 42-57, and for RuO₂ in Figs. 58-60, respectively. In these figures, the peak position is indicated in eV. The binding energies of the core-lines are summarized in Tables 1-5 and the kinetic energies of the Auger lines are listed in Table 6.

4.2 Metal surfaces

The binding energies of the core-lines for Y_{*et*}, Zr_{*et*}, and Nb_{*et*} shifted to the higher binding energy side by 0.1-1.0 eV from those for the corresponding metallic surfaces obtained by mechanical filing. These core-line shifts have been observed in such metals as Pd,³⁾ Ti,¹⁾ and V.¹⁾

The kinetic energies of the Auger-lines for Y_{et} , Zr_{et} and Nb_{et} also shifted to the lower kinetic energy side by 0.9-1.7 eV. It is apparent that these energy shifts are not due to the surface oxides, since the spectral intensity of the O1s area remained unchanged after the Ar^+ ion bombardment.

One of the plausible reasons of the energy shifts may be the radiation damage induced by the Ar^+ ion bombardment. In fact, it has been observed that the bombardment with heavy-ions causes the surface roughness such as cone formation.⁴⁻⁶⁾ Although the quantitative explanation of the ion-induced damages has not been given, an importance of the nucleation and growth of the vacancy clusters in the surface layer was pointed out.^{7,8)} In this model, the ion-induced vacancies in the surface layer agglomerate by diffusion resulting in the formation of the porous metal surfaces.

On the other hand, the core-line energies seem to be related to the atomic density of the sample. In practice, the binding energies of the gas phase for the transition-metals shift to the higher energy side by 2-4 eV from those of the solid phase.^{9,10)} Thus, the core-line shift to the higher energy side for the ion bombarded metal is presumably associated with the formation of the porous surfaces whose atomic density is relatively small compared with the original metals. To confirm this assumption, we have measured the XPS spectra for porous Nb metal obtained by the following procedure.

First, the niobium hydride $NbH_{0.86}$ was thermally synthesized in the electric furnace by the direct reaction of Nb metal with hydrogen at $570^\circ C$. The hydride was then dehydrogenated at $1100^\circ C$ under the high vacuum. By this treatment, the $Nb3d_{5/2}$ line was moved to 202.6 eV, which is higher by 0.2 eV than that for Nb_{fl} . Since there exists no phase transition of Nb metal below the melting point, i.e., $2400^\circ C$,¹¹⁾ the dehydrogenated Nb metal may preserve the crystal structure of hydride. The phenomenon is similar to the result of the Ar^+ ion bombarded surfaces, though the energy shift is smaller compared with that for Nb_{et} . Such an energy discrepancy between dehydrogenated and filed metals was also observed for vanadium system. The $V2p_{3/2}$ line for dehydrogenated vanadium appears at 512.4 eV, which is higher by 0.3 eV from that for V_{fl} .

Considering the results mentioned above, it should be careful to use the data for the sputtered surface as an energy reference of chemical

shifts in such metals as Ti,¹⁾ V,¹⁾ Y, Zr, and Nb. On the other hand, the energy shifts were not observed in Sc,¹⁾ Ni,¹⁾ and Mo, upto the total fluence of $\sim 10^{18}$ ions/cm². In the present stage, we cannot give conclusive explanation to the present results that the energy shift of the Ar⁺ ion bombarded Nb metal is the largest in all the metals examined. However, it is evident that the metals which give appreciable energy shifts are those easily absorbing hydrogen to form relatively stable hydride and having the porous metal structure after dehydrogenation.

4. 3 Oxides

The binding energies or the chemical shifts of the main core-lines are almost same as those previously reported for Y₂O₃,¹²⁾ ZrO₂,¹²⁾ Nb₂O₅,¹²⁻¹⁵⁾ and MoO₃.^{12,16-18)}

Although the chemical shifts of the Auger lines had long been considered to be almost same as those of the corresponding core-lines, it has been found that these two energy shifts are often different because of difference in the extra-atomic relaxation energy.¹⁰⁾ The separation between the Auger line and the core-line reflects the extra-atomic relaxation energy. This has been called the Auger parameter α ,¹⁰⁾ and defined as a following equation,

$$\begin{aligned}\alpha &= KE_A - KE_p \\ &= KE_A + BE_p - h\nu\end{aligned}$$

where KE and BE represent the kinetic energy and the binding energy, the suffix A and p represent the Auger electron and photoelectron, respectively, and $h\nu$ is the exciting X-ray energy. Using the Auger parameter, the charging effect which is often observed in the spectroscopic measurements of the insulating samples can be canceled. Another experimental advantage of the use is that the correction of the work function is not necessary, and the measured values can be directly compared with those obtained by the other investigators.

The Auger parameters for the oxides and their shifts from those of the

metallic states obtained by the mechanical filing are given in Table 7. In Nb and Mo system, the large chemical shifts of both the $3d_{5/2}$ lines and $M_{4,5} N_{2,3} V$ Auger lines are canceled. Since $\Delta\alpha$ from the metallic state decreases with the polarization of the chemical bond,¹⁰⁾ the values for Nb_2O_5 and MoO_3 indicate the large polarization of the metal-O bonds in these oxides.

REFERENCES

- 1) Baba Y. and Sasaki T. A. : JAERI-M 84-005, Japan Atomic Energy Research Institute (1984).
- 2) Wagner C. D., Riggs W. M., Davis L. E., Moulder J. F. and Mullenberg G. E. : "Handbook of X-ray Photoelectron Spectroscopy", Perkin-Elmer Corporation, Minnesota (1979).
- 3) Hufner S., Wertheim G. K. and Buchanan D. N. E. : Chem. Phys. Lett., 24, 527 (1974).
- 4) Wehner G. K. and Hajicek D. J. : J. Appl. Phys., 42, 1145 (1971).
- 5) Tsunoyama K., Suzuki T. and Ohashi Y. : Japanese J. Appl. Phys., 15, 349 (1976).
- 6) Bhatia C. S. : Thin Solid Films, 96, 249 (1982).
- 7) Cherns D. : Phil. Mag., 36, 1429 (1977).
- 8) Verheij L. K., Van den Berg J. A. and Armour D. G. : Surf. Sci., 122, 216 (1982).
- 9) Ley L., Kowalczyk S. P., McFeely F. R., Pollak R. A. and Shirley D. A. : Phys. Rev. B, 8, 3583 (1973).
- 10) Wagner C. D. : Faraday Discuss. Chem. Soc., 60, 291 (1975).
- 11) For example see Miller G. L. : "Tantalum and Niobium", Butterworths Scientific Publication, London (1959), p372.
- 12) Nefedov V. I., Gati D., Dzhurinskii B. F., Sergushin N. P. and Salyn Ya. V. : Zh. Neorg. Khim., 20, 2307 (1975).
- 13) McGuire G. E., Schweitzer G. K. and Carlson T. A. : Inorg. Chem., 12, 2451 (1973).
- 14) Simon D., Perrin C. and Baillif P. : C. R. Acad. Sci. Paris, C 241, 283 (1976).
- 15) Fontaine R., Cailiat R., Feve L. and Guittet M. J. : J. Electron Spectrosc., 10, 349 (1977).
- 16) Grim S. O. and Matienzo L. J. : Inorg. Chem., 14, 1015 (1975).
- 17) Patterson T. A., Carver J. C., Leyden D. E. and Hercules D. M. : J. Phys. Chem., 80, 1702 (1976).
- 18) Ivanov I. K., Kostikov Yu. P., Korol'kov D. V. and Avramekov A. G. : Zh. Obshch. Khim., 47, 1189 (1977).

Table 1 Binding energies and chemical shifts of the core-lines for Y_{fl} , Y_{et} and Y_2O_3 .

Sample	Orbital	E_b (eV)	Chemical Shift (eV)	Fig. No.
Y_{fl}	3s	395.4	-	3
	$3p_{3/2}$	299.3	-	4
	$3d_{3/2}$	157.9	-	5
	$3d_{5/2}$	155.9	-	5
	4p	24.1	-	6
Y_{et}	$3d_{3/2}$	158.2	0.3	9
	$3d_{5/2}$	156.1	0.2	9
Y_2O_3	3s	396.1	0.7	11
	$3p_{3/2}$	301.6	2.3	12
	$3d_{3/2}$	160.5	2.6	13
	$3d_{5/2}$	158.6	2.7	13

Table 2 Binding energies and chemical shifts of the core-lines for Zr_{fl} , Zr_{et} and ZrO_2 .

Sample	Orbital	E_b (eV)	Chemical Shift (eV)	Fig. No.
Zr_{fl}	3s	430.2	-	17
	$3p_{3/2}$	329.9	-	18
	$3d_{3/2}$	181.4	-	19
	$3d_{5/2}$	179.0	-	19
	4p	27.5	-	20
Zr_{et}	$3d_{3/2}$	181.5	0.1	23
	$3d_{5/2}$	179.2	0.2	23
ZrO_2	$3d_{3/2}$	185.5	4.1	25
	$3d_{5/2}$	183.3	4.3	25

Table 3 Binding energies and chemical shifts of the core-lines for Nb_{fz} , Nb_{et} and Nb_2O_5 .

Sample	Orbital	E_b (eV)	Chemical Shift (eV)	Fig. No.
Nb_{fz}	3s	467.1	-	29
	3p _{3/2}	360.7	-	30
	3d _{3/2}	205.2	-	31
	3d _{5/2}	202.4	-	31
	4p	31.0	-	32
Nb_{et}	3p _{3/2}	361.7	1.0	35
	3d _{3/2}	205.7	0.5	36
	3d _{5/2}	203.0	0.6	36
Nb_2O_5	3d _{3/2}	210.7	5.5	39
	3d _{5/2}	208.1	5.7	39

Table 4 Binding energies and chemical shifts of the core-lines for Mo_{fz} , Mo_{et} and MoO_3 .

Sample	Orbital	E_b (eV)	Chemical Shift (eV)	Fig. No.
Mo_{fz}	3s	506.3	-	43
	3p _{3/2}	394.0	-	44
	3d _{3/2}	231.1	-	45
	3d _{5/2}	228.0	-	45
	4s	62.6	-	46
	4p	35.6	-	47
Mo_{et}	3d _{3/2}	231.1	0.0	50
	3d _{5/2}	227.9	-0.1	50
MoO_3	3s	511.0	4.7	52
	3p _{3/2}	398.6	4.6	53
	3d _{3/2}	235.8	4.7	54
	3d _{5/2}	232.7	4.7	54
	4p	40.4	4.8	55

Table 5 Binding energies of the core-lines for RuO₂.

Orbital	E _b (eV)	Fig. No.
3p _{3/2}	463.0	58
3d _{3/2}	285.4	59
3d _{5/2}	281.2	59

Table 6 Kinetic energies and chemical shifts of the M_{4,5}N_{2,3}^V Auger lines for Y, Zr, Nb, Mo and their compounds.

Sample	E _k (eV)	Chemical Shift (eV)	Fig. No.
Y _{fl}	124.3	-	8
Y _{et}	123.4	0.9	10
Y ₂ O ₃	117.8	6.5	15
Zr _{fl}	148.6	-	22
Zr _{et}	147.3	1.3	24
ZrO ₂	141.9	6.7	27
Nb _{fl}	167.8	-	34
Nb _{et}	166.1	1.7	38
Nb ₂ O ₅	161.6	6.2	41
Mo _{fl}	187.0	-	49
Mo _{et}	187.1	-0.1	51
MoO ₃	182.0	5.0	57

Table 7 Auger parameters and their shifts from metallic states for Y, Zr, Nb, Mo and their oxides.

Sample	α (eV)	$\Delta\alpha$ (eV)
Y	-973.4	-
Y ₂ O ₃	-977.2	3.8
Zr	-926.0	-
ZrO ₂	-928.4	2.4
Nb	-883.4	-
Nb ₂ O ₅	-883.9	0.5
Mo	-838.6	-
MoO ₃	-838.9	0.3

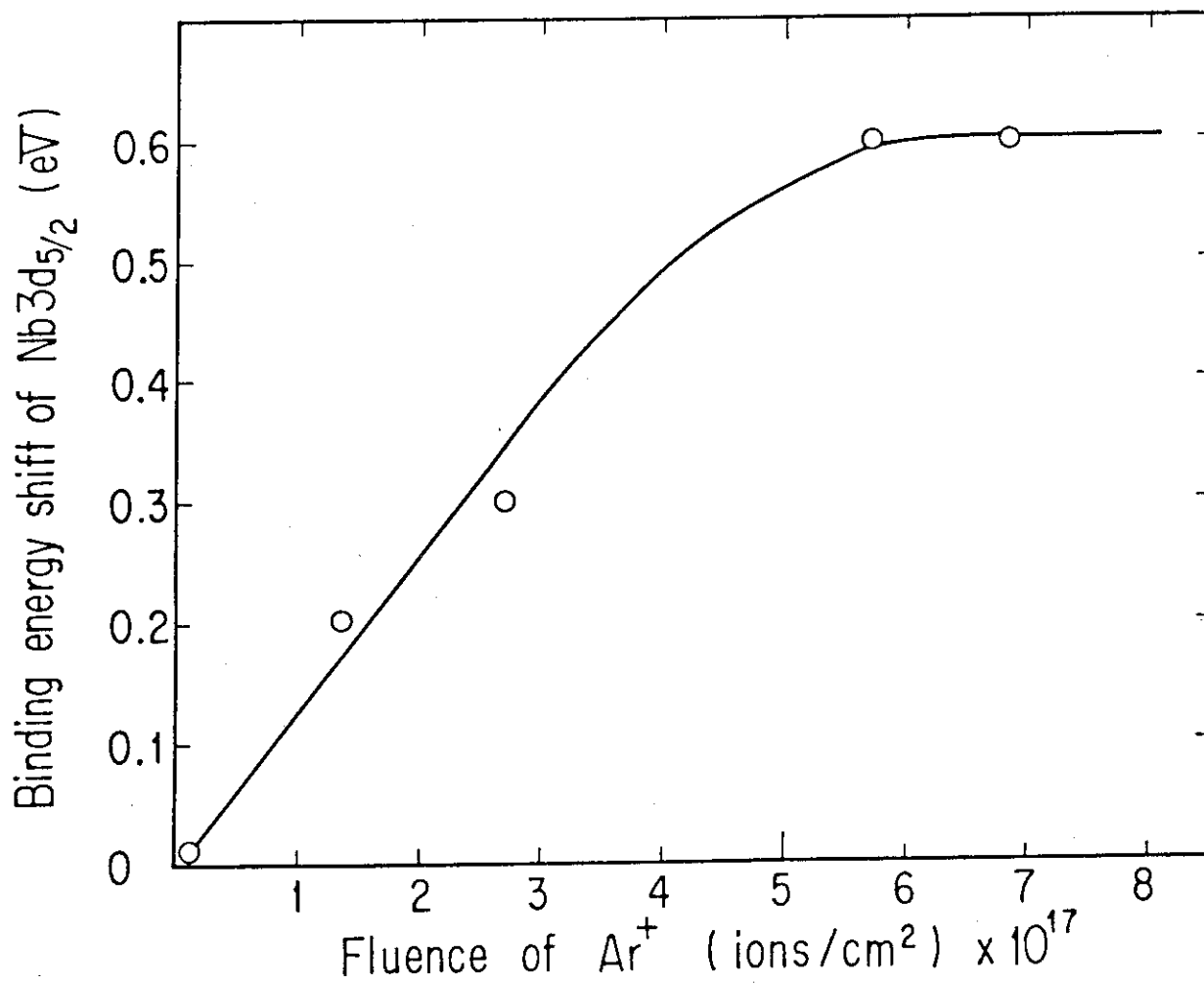


Fig. 1 Binding energy shifts of Nb_{3d_{5/2}} line for Ar⁺ ion bombarded Nb metal as a function of ion fluence.

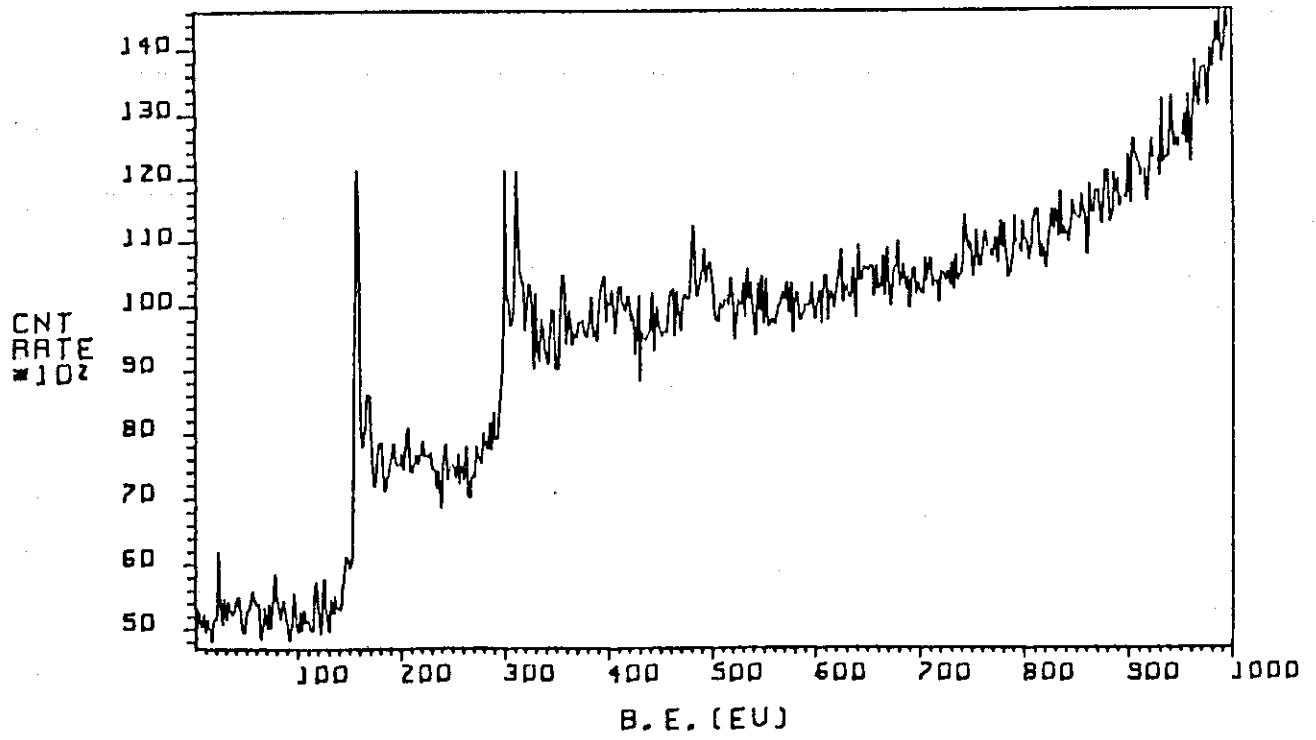


Fig. 2 XPS wide scan of Y_{fz} .

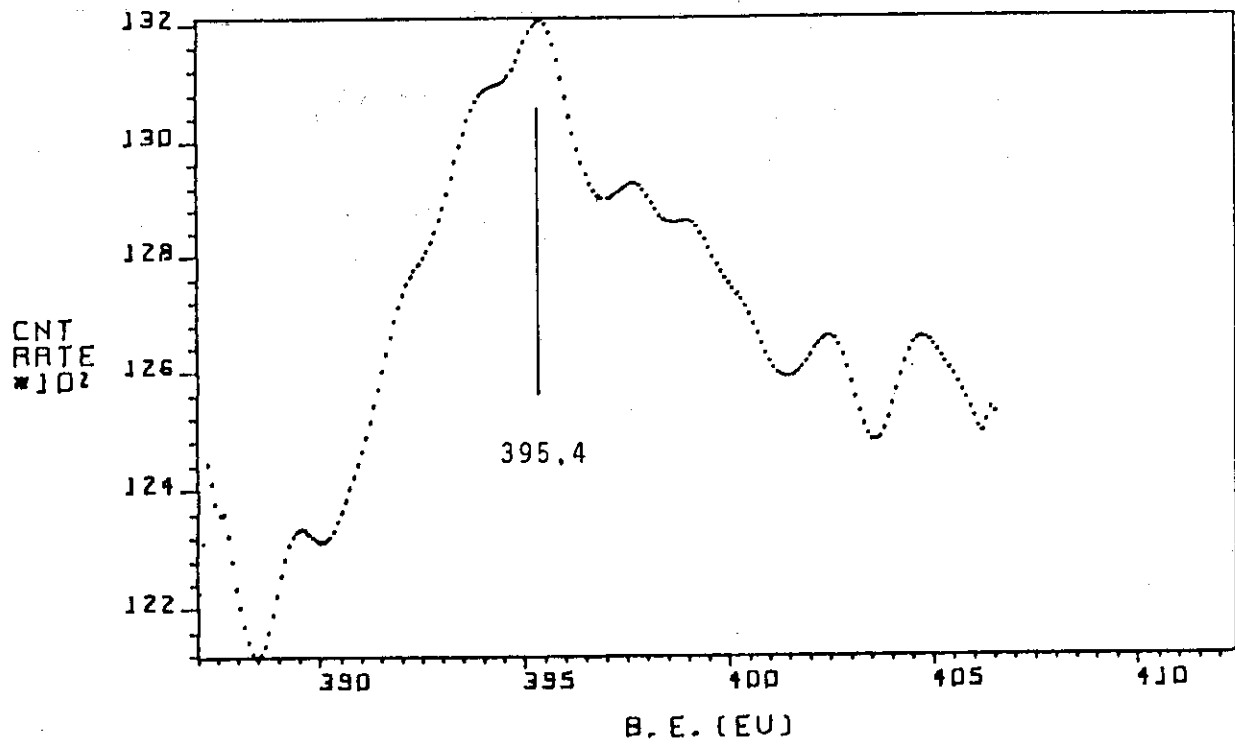


Fig. 3 Y_{3s} XPS spectrum of Y_{fz} .

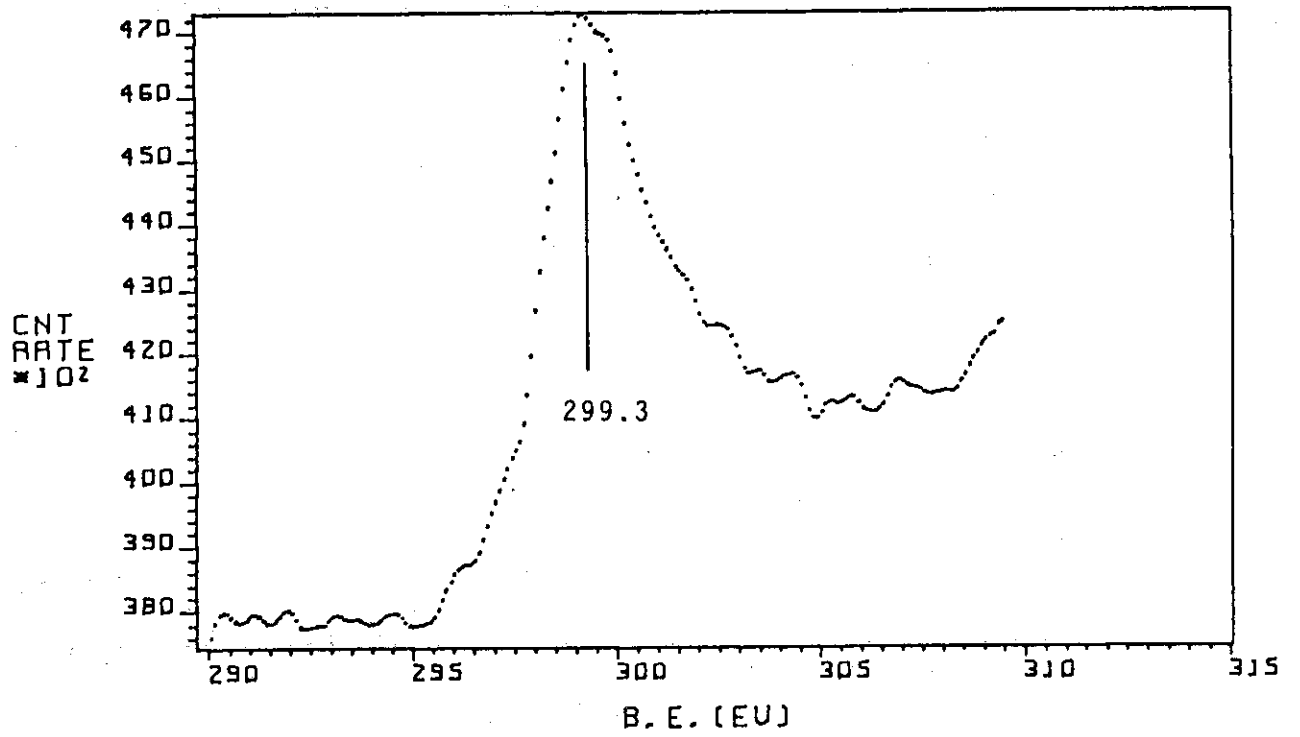


Fig. 4 Y_{3p} XPS spectrum of Y_{fl}.

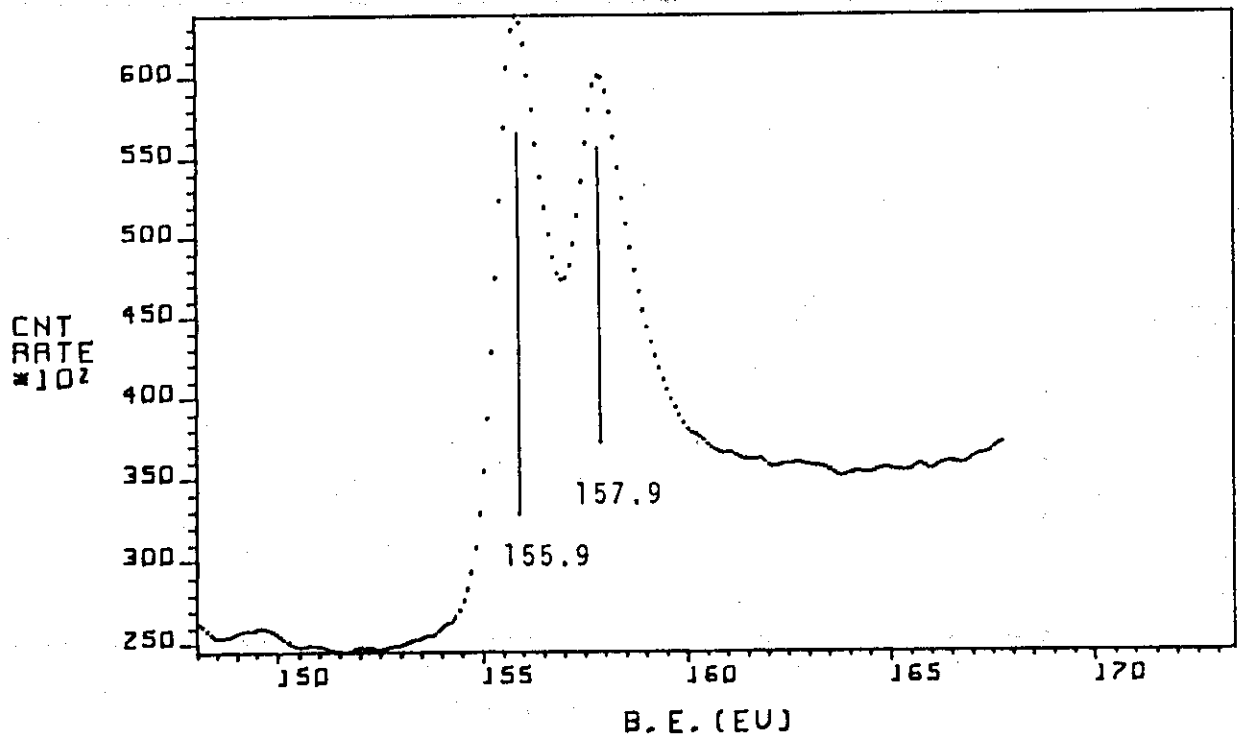


Fig. 5 Y_{3d} XPS spectrum of Y_{fl}.

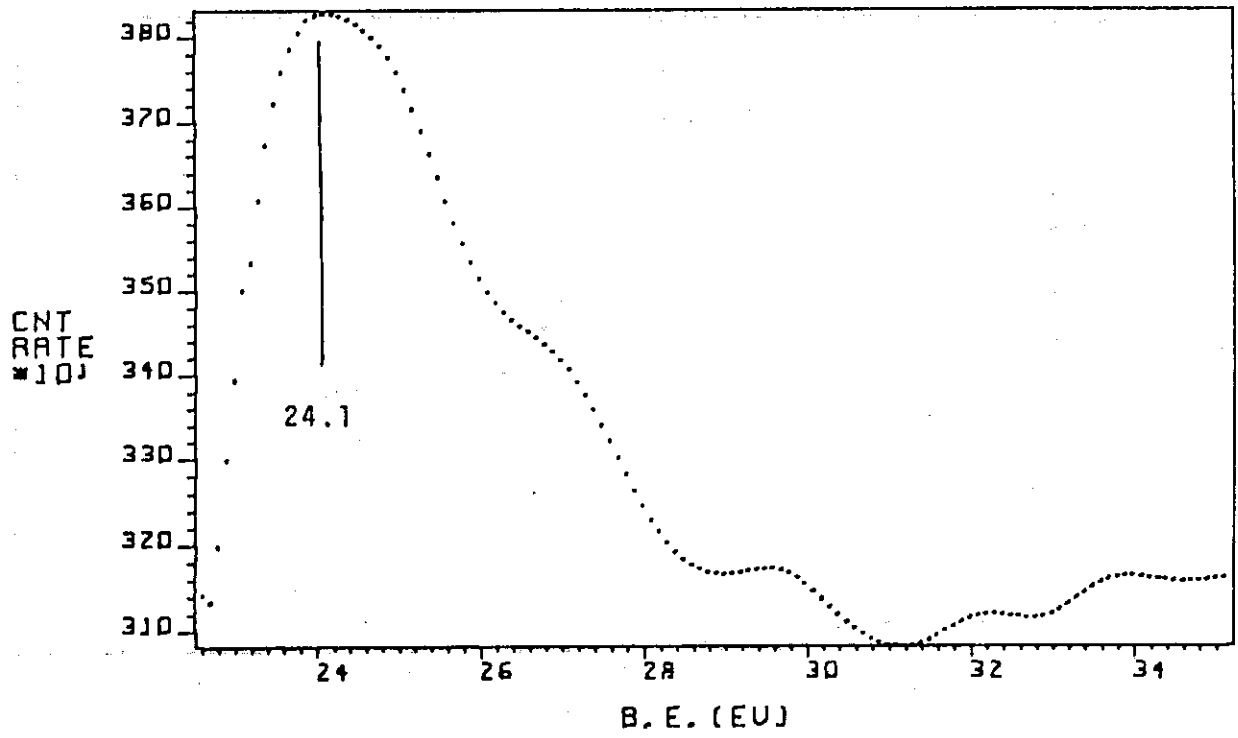


Fig. 6 Y_{4p} XPS spectrum of Y_{fl}.

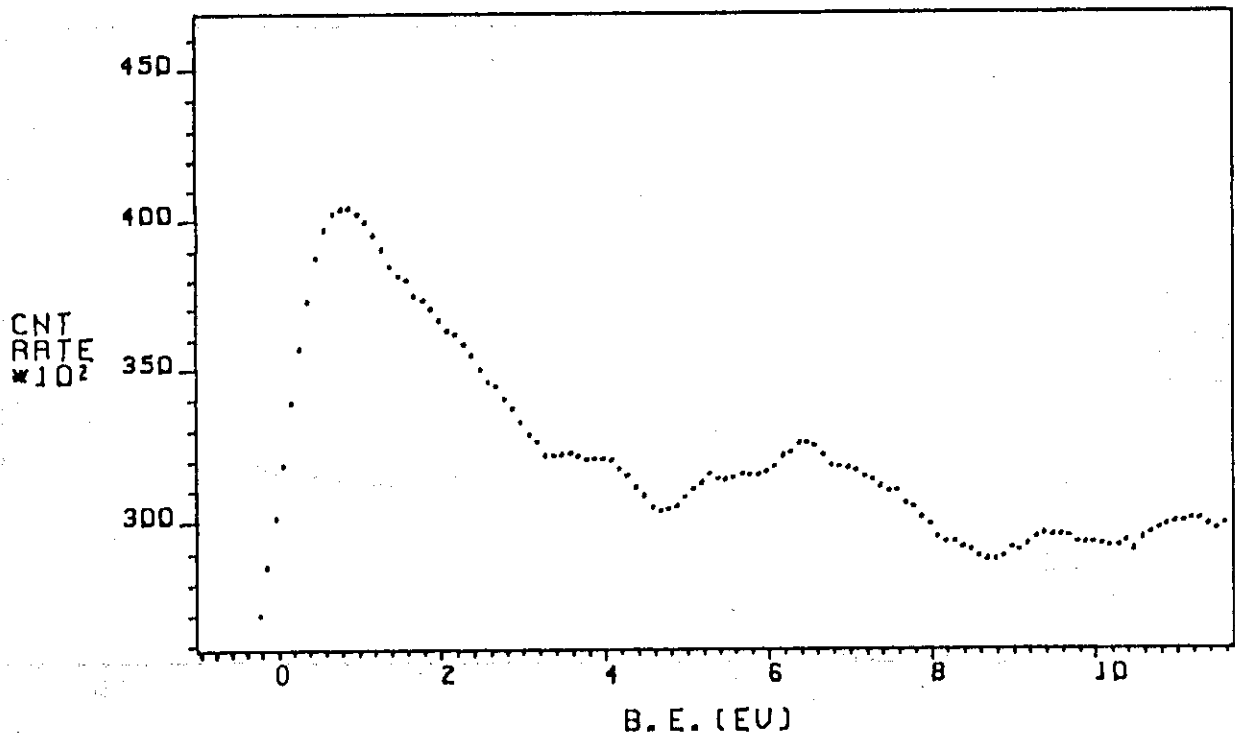


Fig. 7 Valence-band spectrum of Y_{fl}.

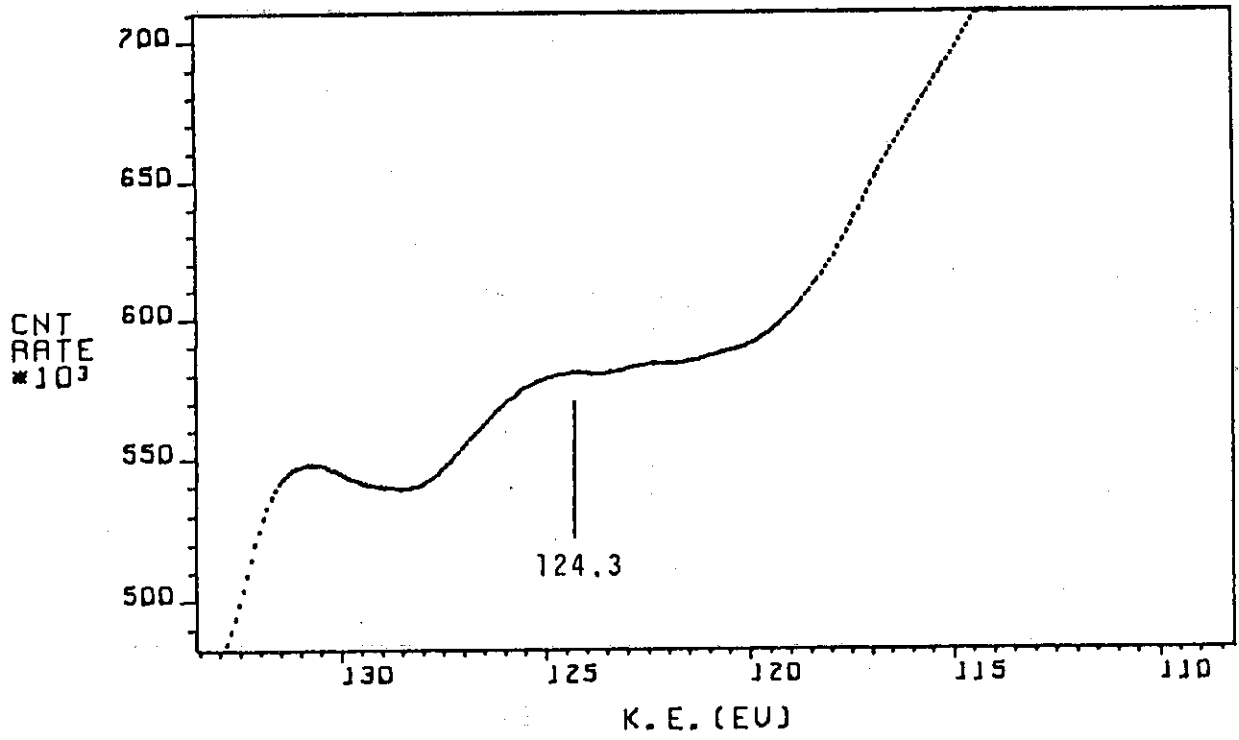


Fig. 8 $M_{4,5}N_{2,3}V$ XAES spectrum of Y_{fz} .

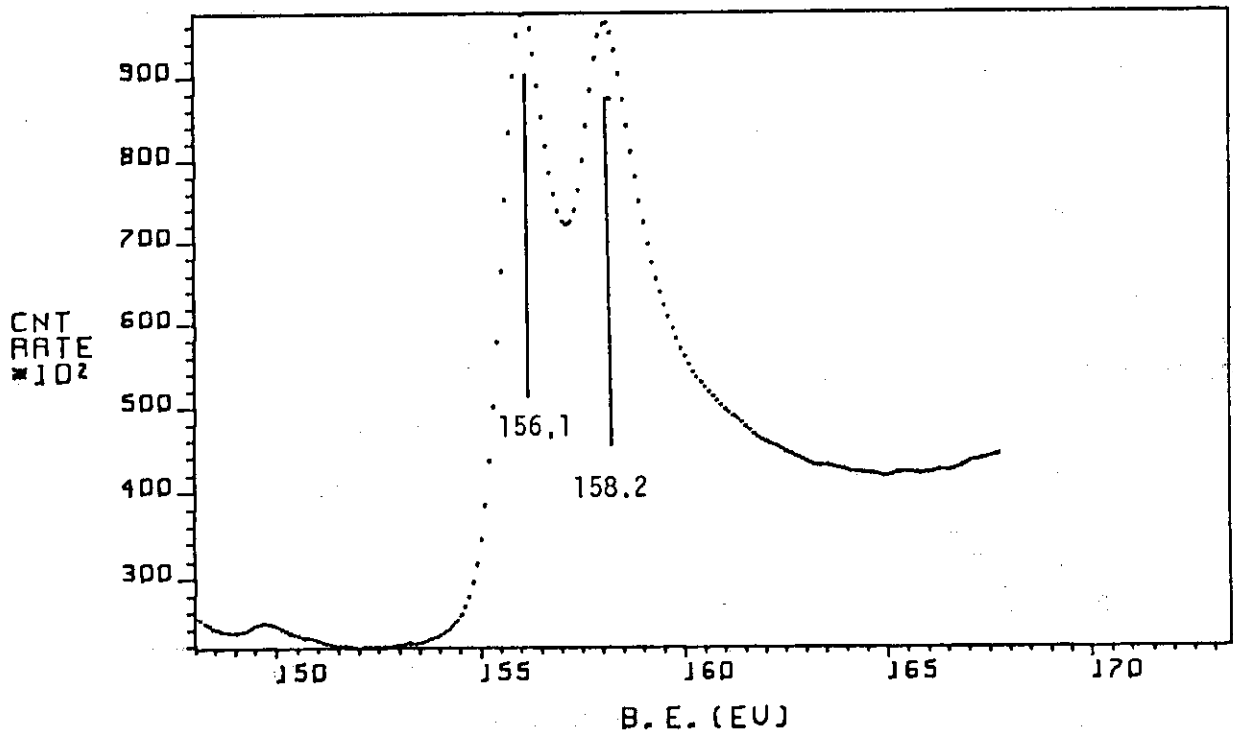


Fig. 9 Y_{3d} XPS spectrum of Y_{et} .

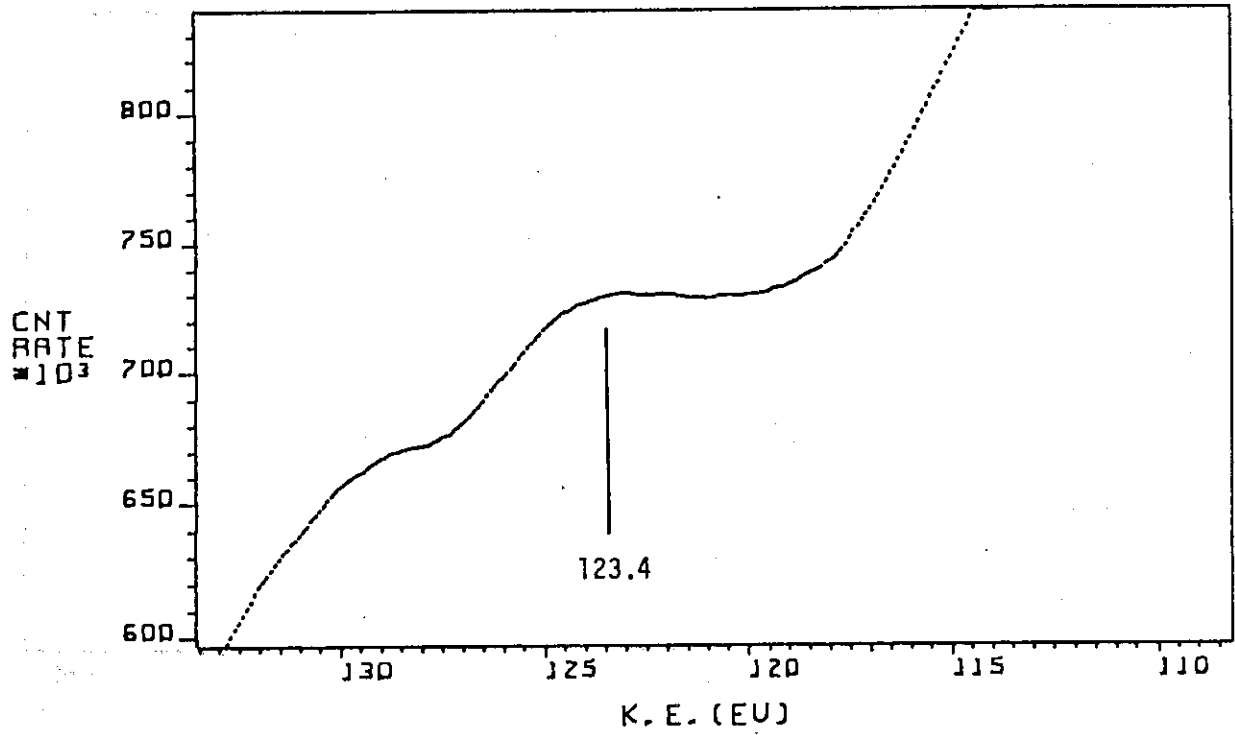


Fig. 10 $M_{4,5}N_{2,3}V$ XAES spectrum of Y_{et} .

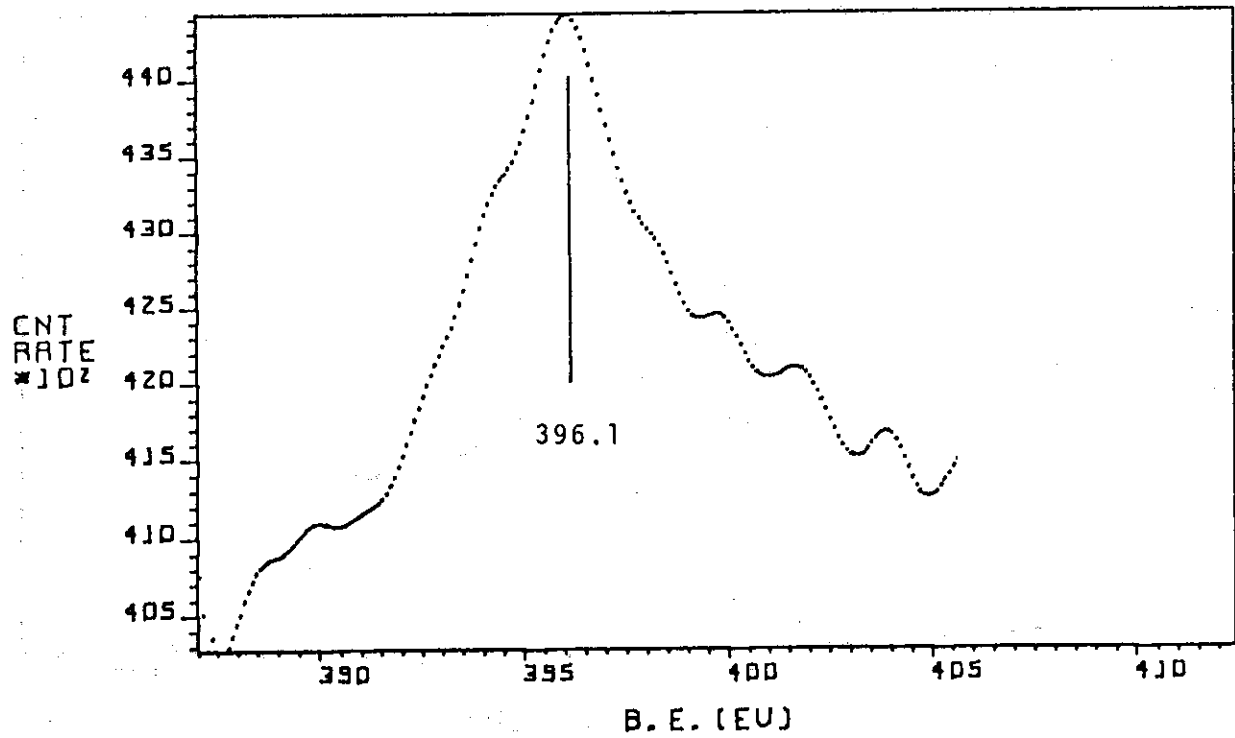


Fig. 11 Y_{3s} XPS spectrum of Y_2O_3 .

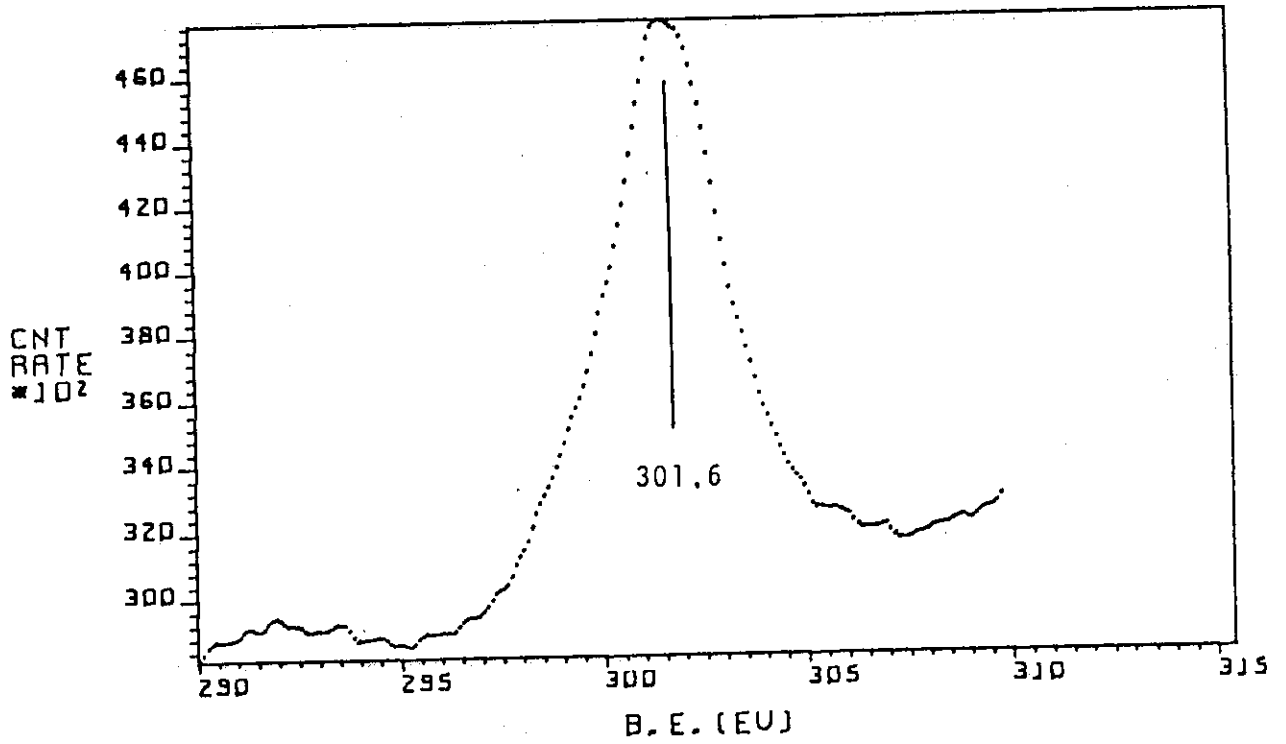


Fig. 12 Y_{3p} XPS spectrum of Y₂O₃.

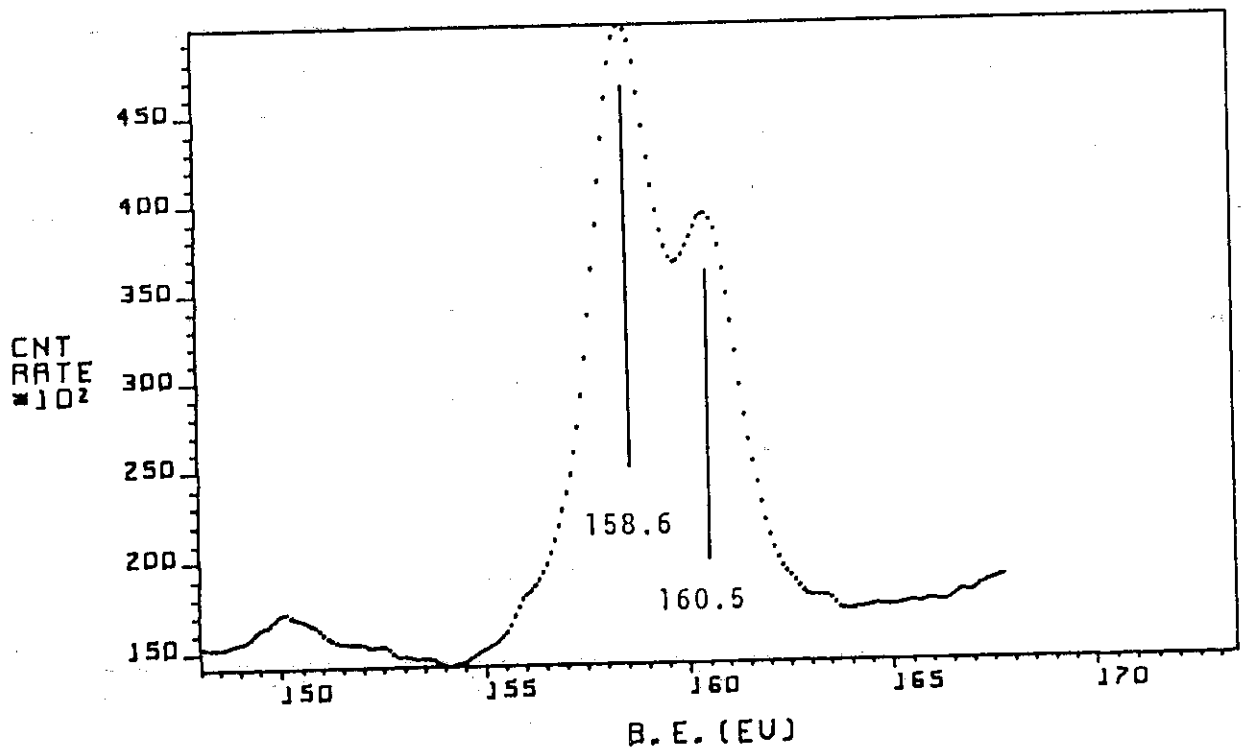


Fig. 13 Y_{3d} XPS spectrum of Y₂O₃.

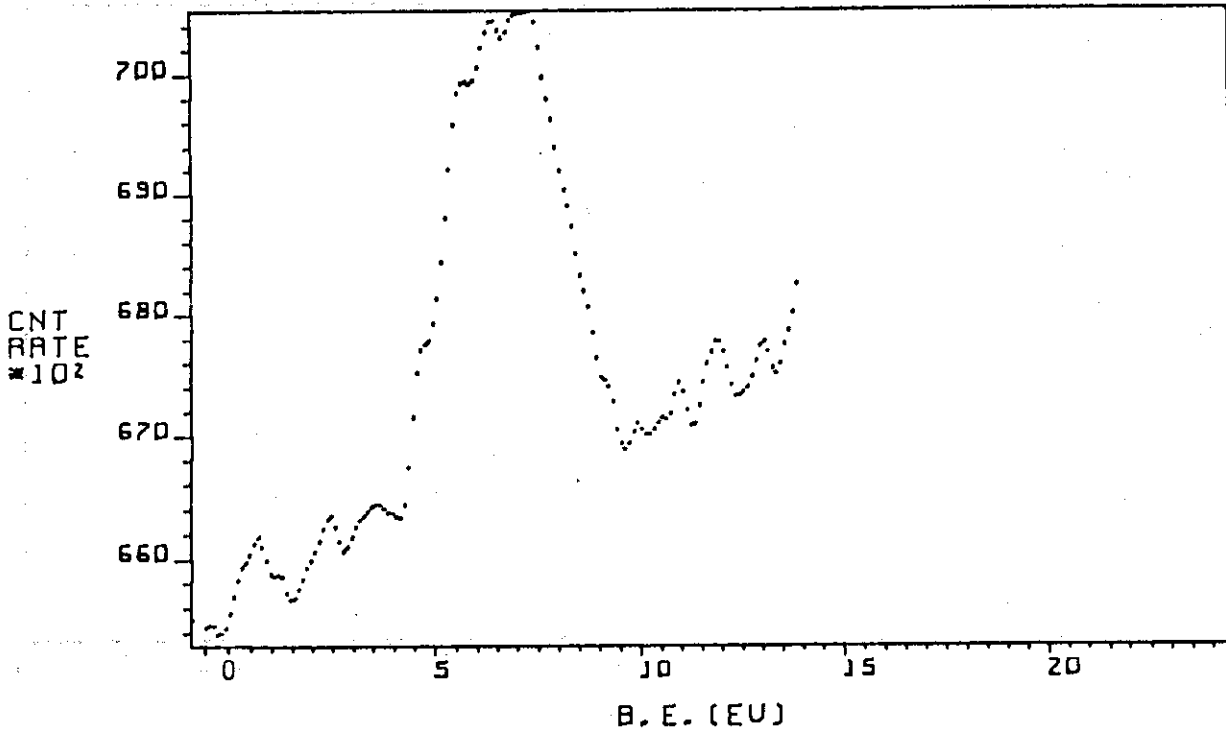


Fig. 14 Valence-band spectrum of Y₂O₃.

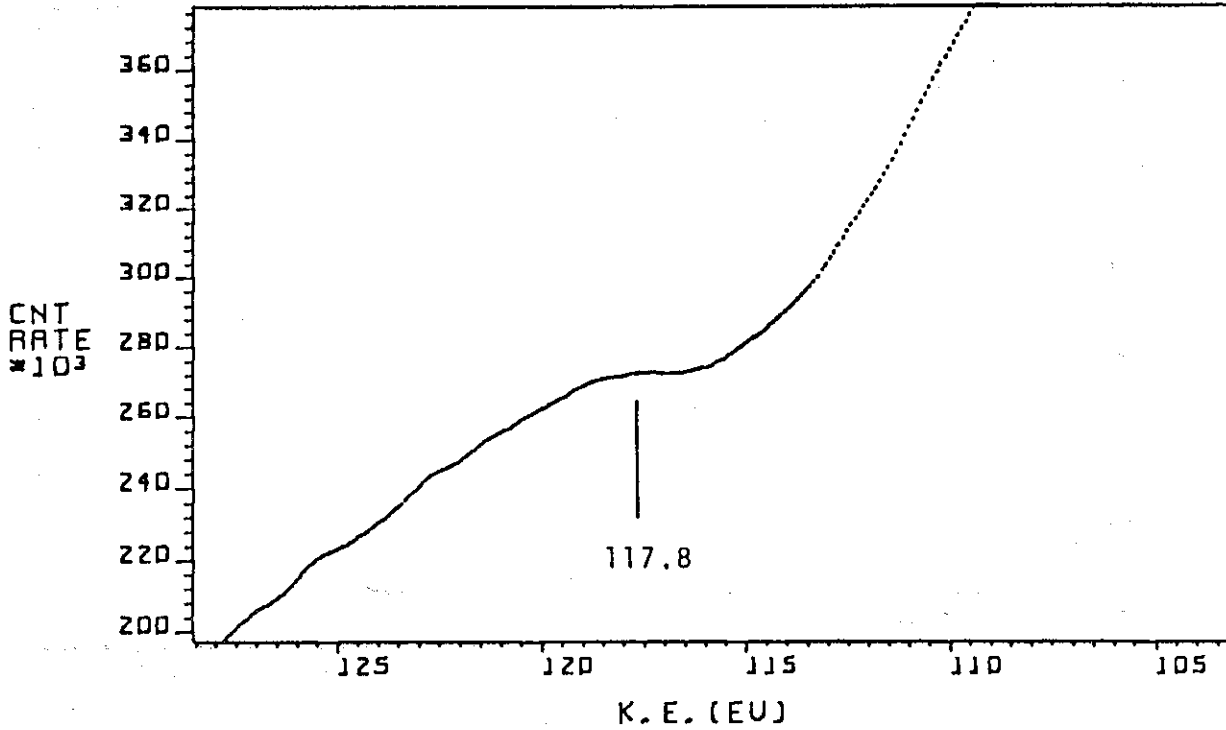


Fig. 15 M_{4,5}N_{2,3}V XAES spectrum of Y₂O₃.

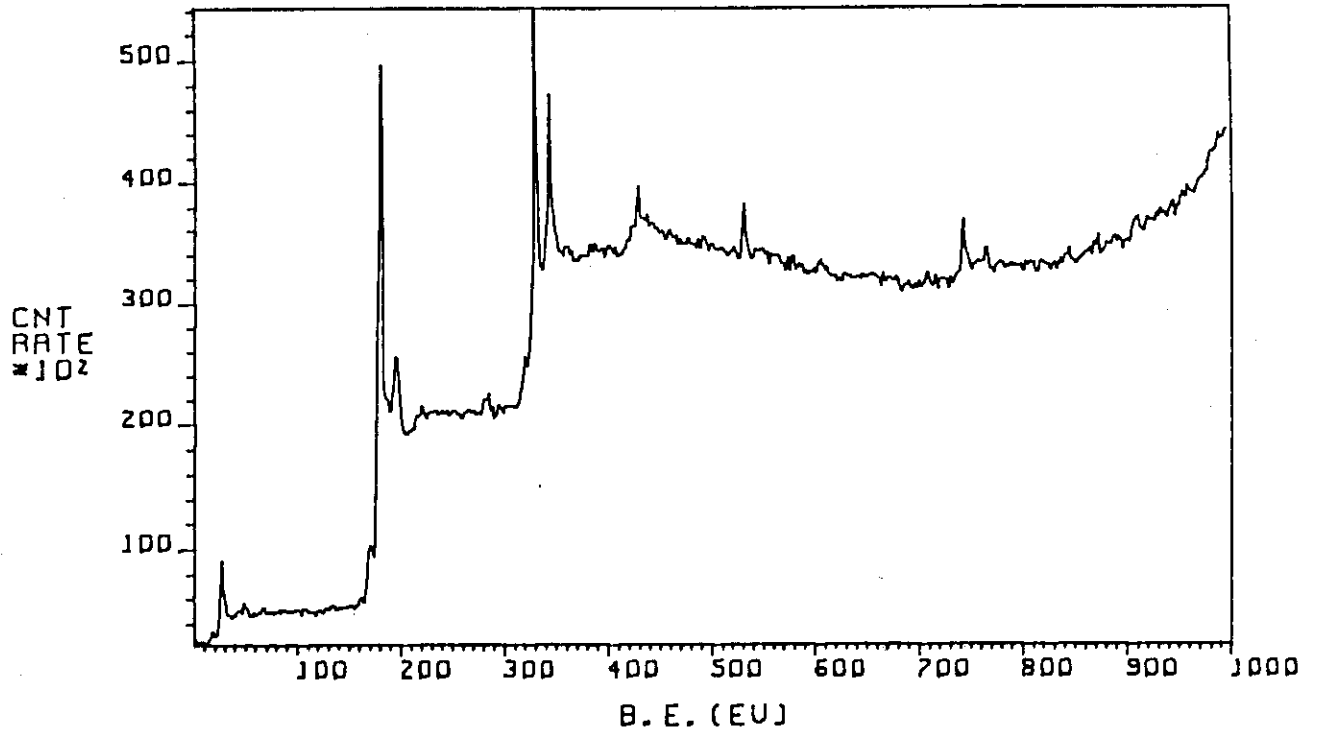


Fig. 16 XPS wide scan of Zr_{fl} .

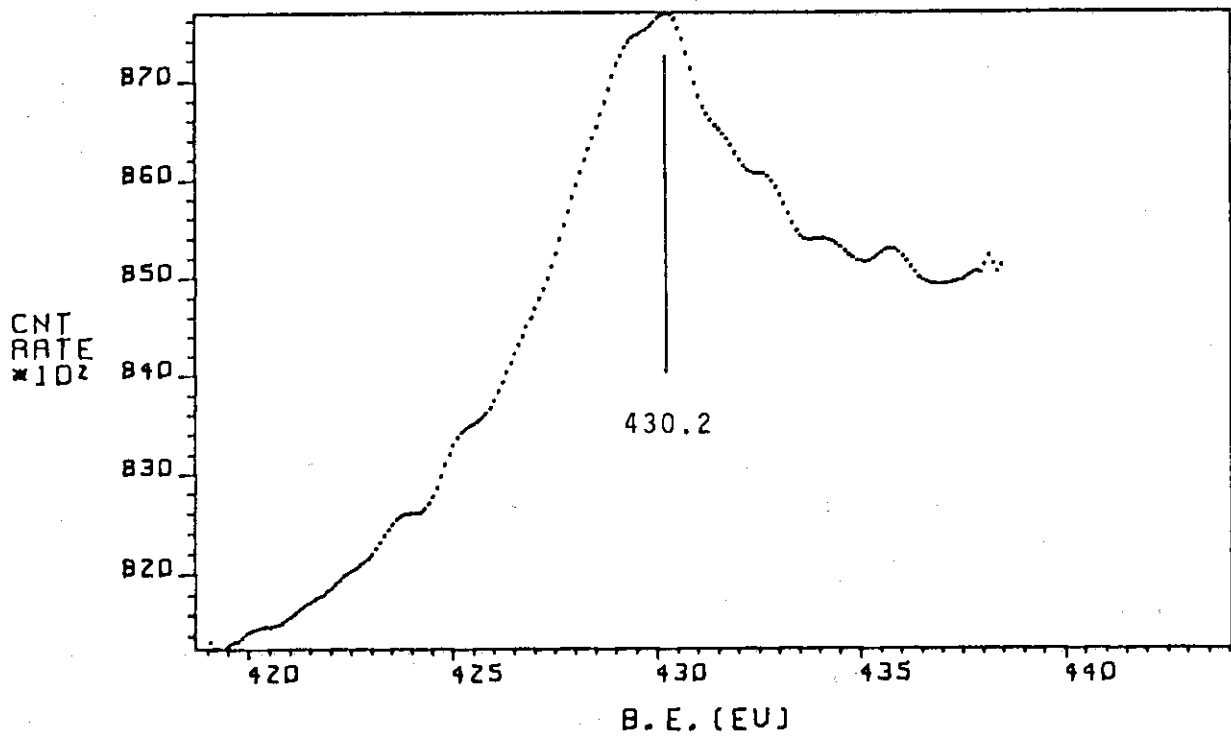


Fig. 17 Zr_{3s} XPS spectrum of Zr_{fl} .

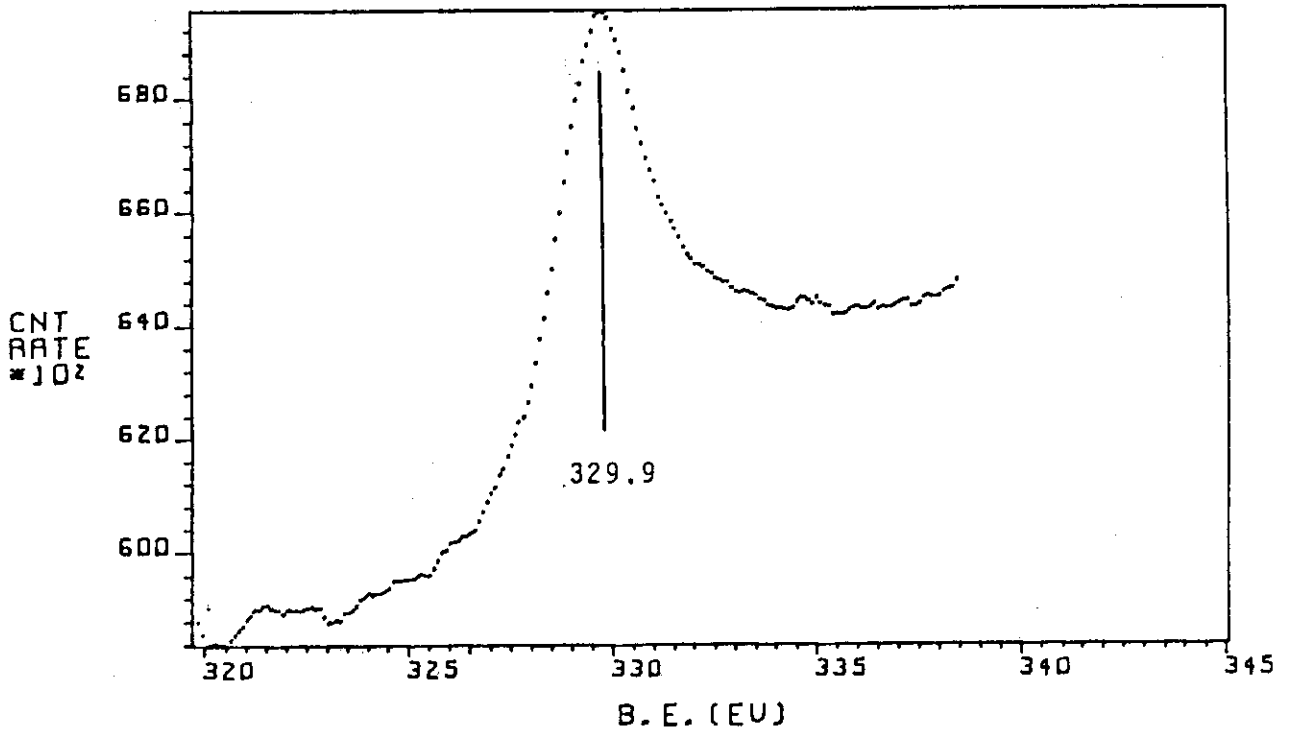


Fig. 18 Zr3p XPS spectrum of Zr_{fl}.

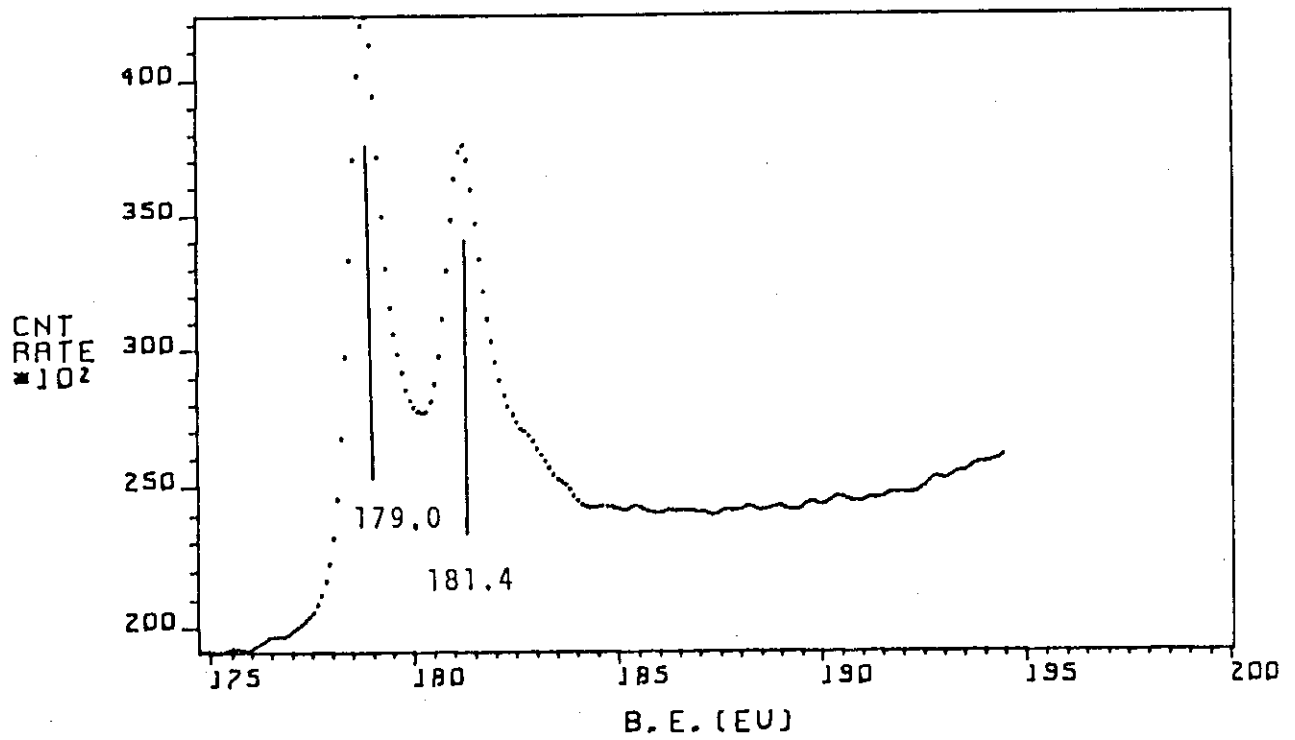


Fig. 19 Zr3d XPS spectrum of Zr_{fl}.

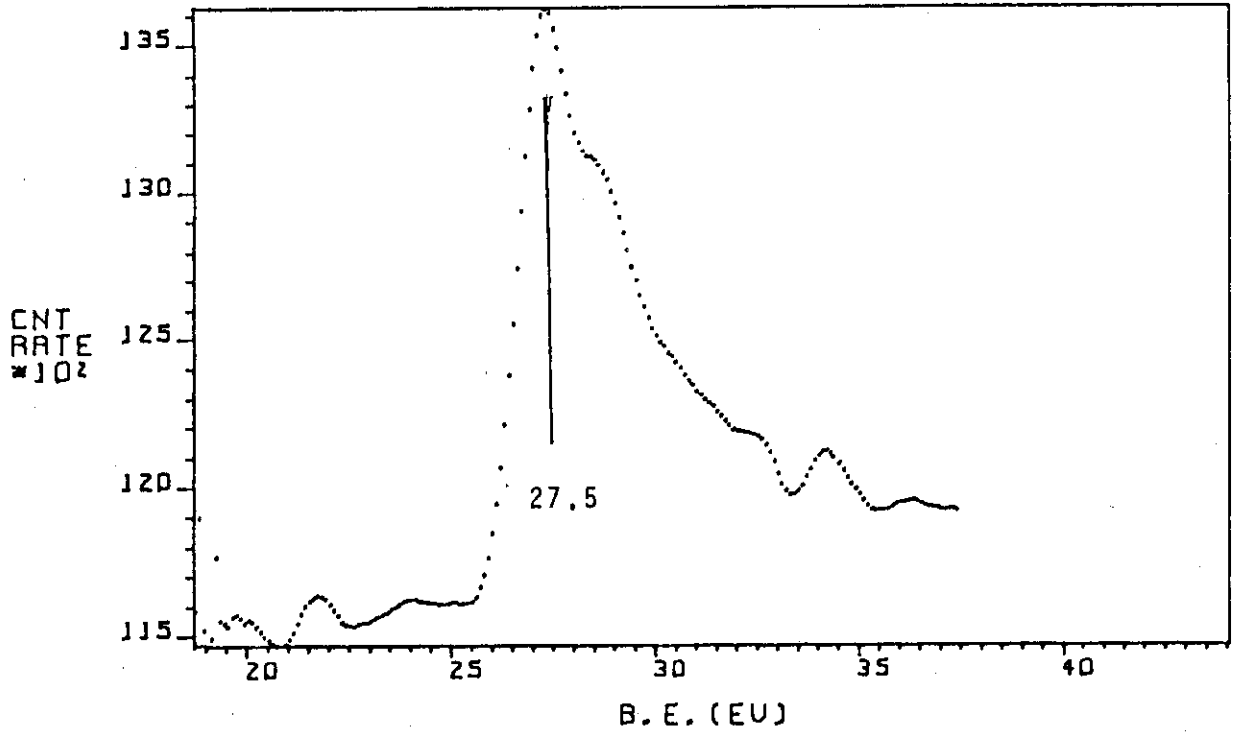


Fig. 20 Zr_{4p} XPS spectrum of Zr_{fl}.

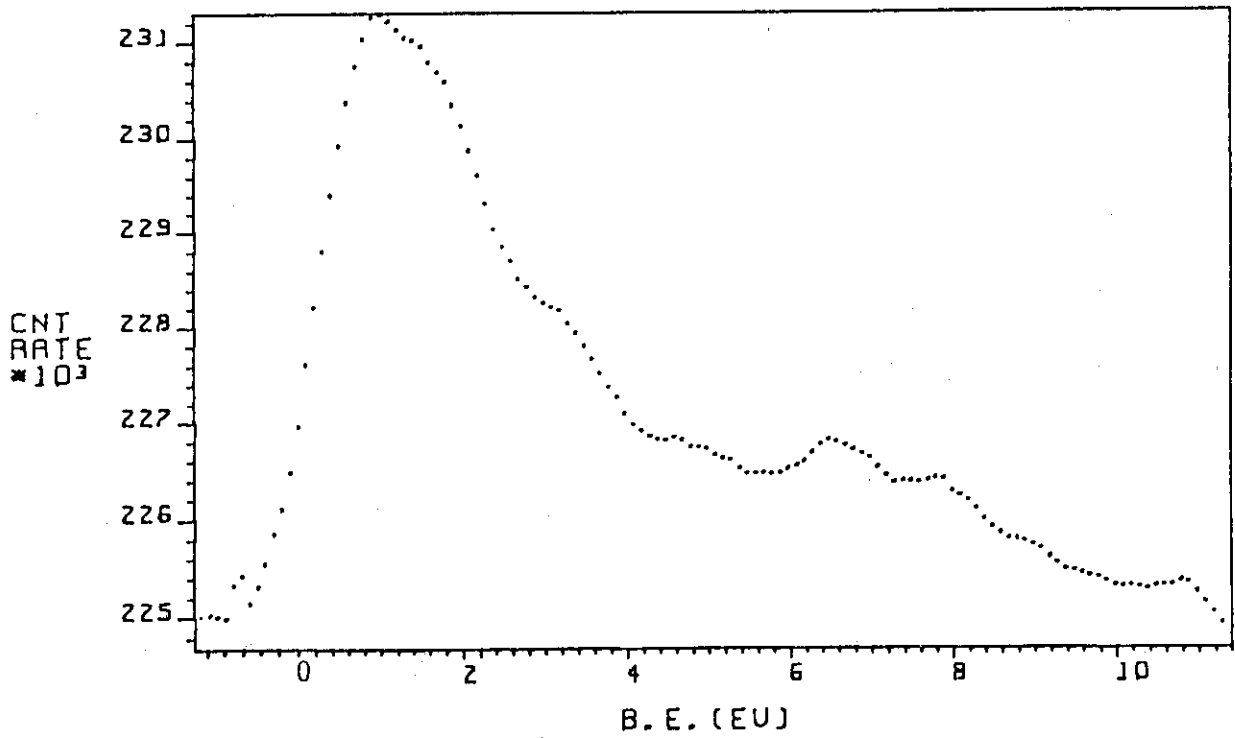


Fig. 21 Valence-band spectrum of Zr_{fl}.

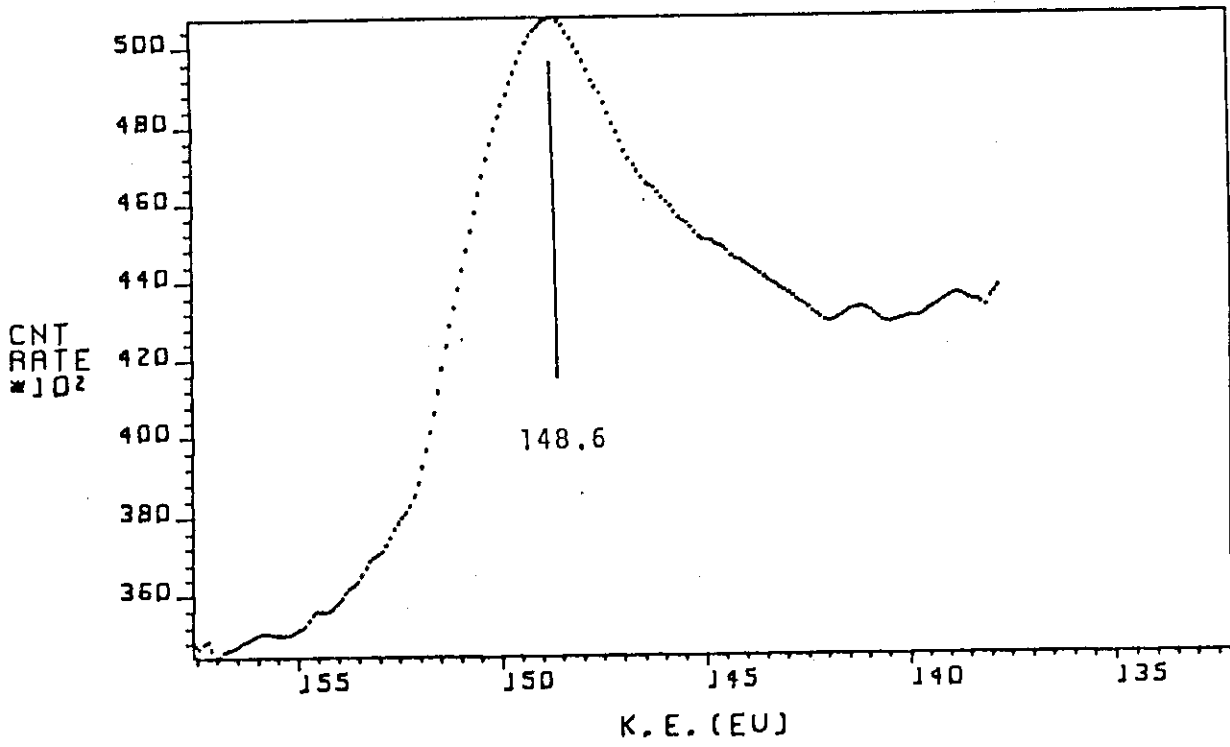


Fig. 22 $M_{4,5}N_{2,3}V$ XAES spectrum of Zr_{fl} .

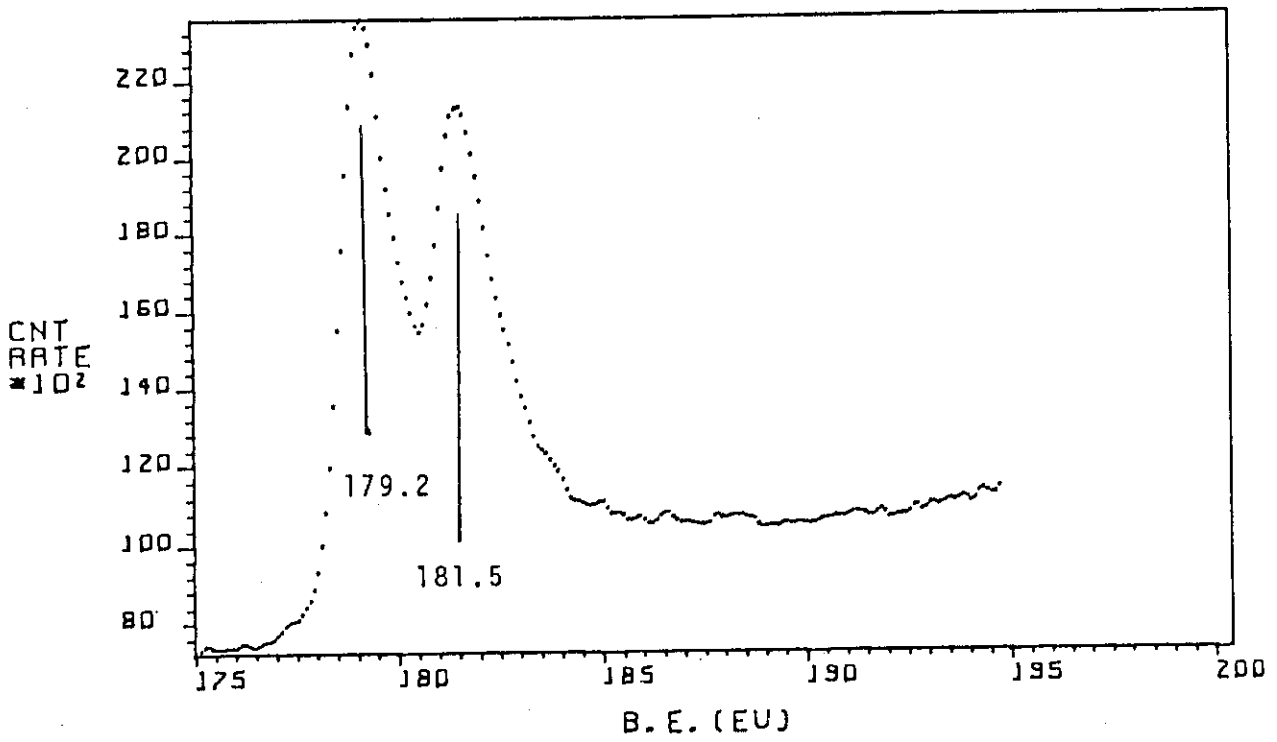


Fig. 23 Zr_{3d} XPS spectrum of Zr_{et} .

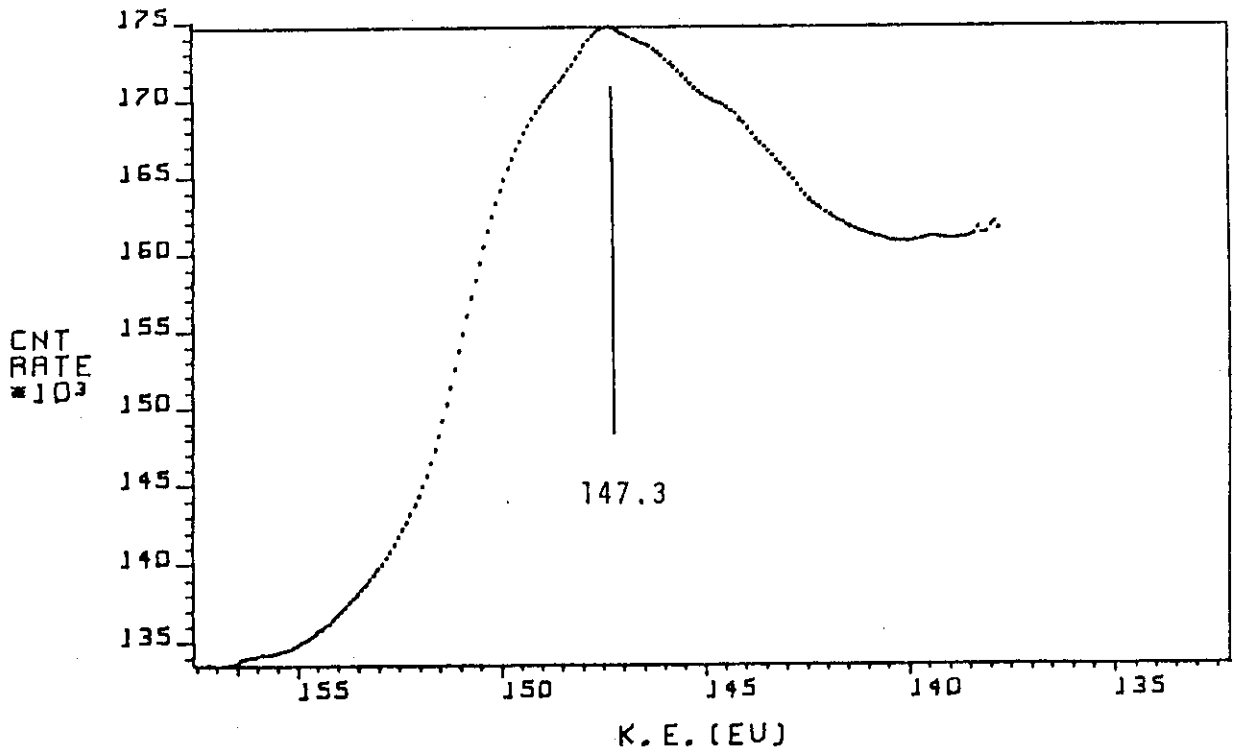


Fig. 24 $M_{4,5}N_{2,3}V$ XAES spectrum of Zr_{et} .

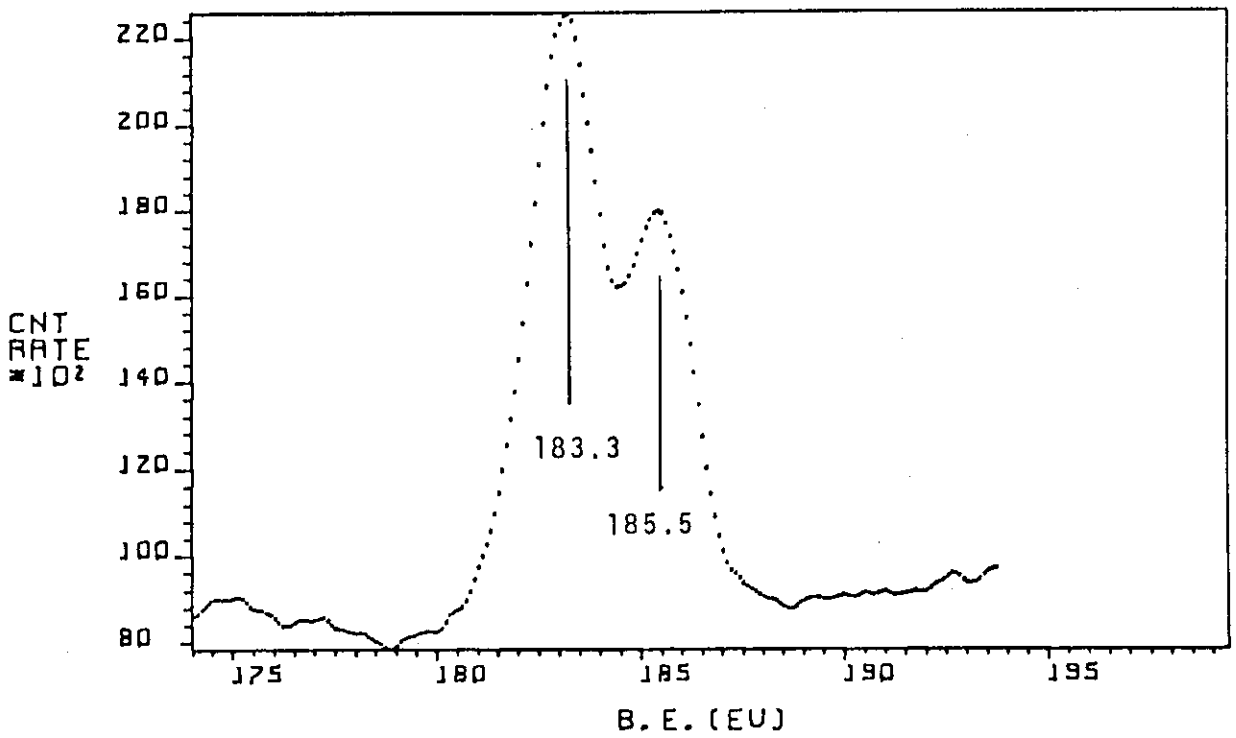


Fig. 25 Zr_{3d} XPS spectrum of ZrO_2 .

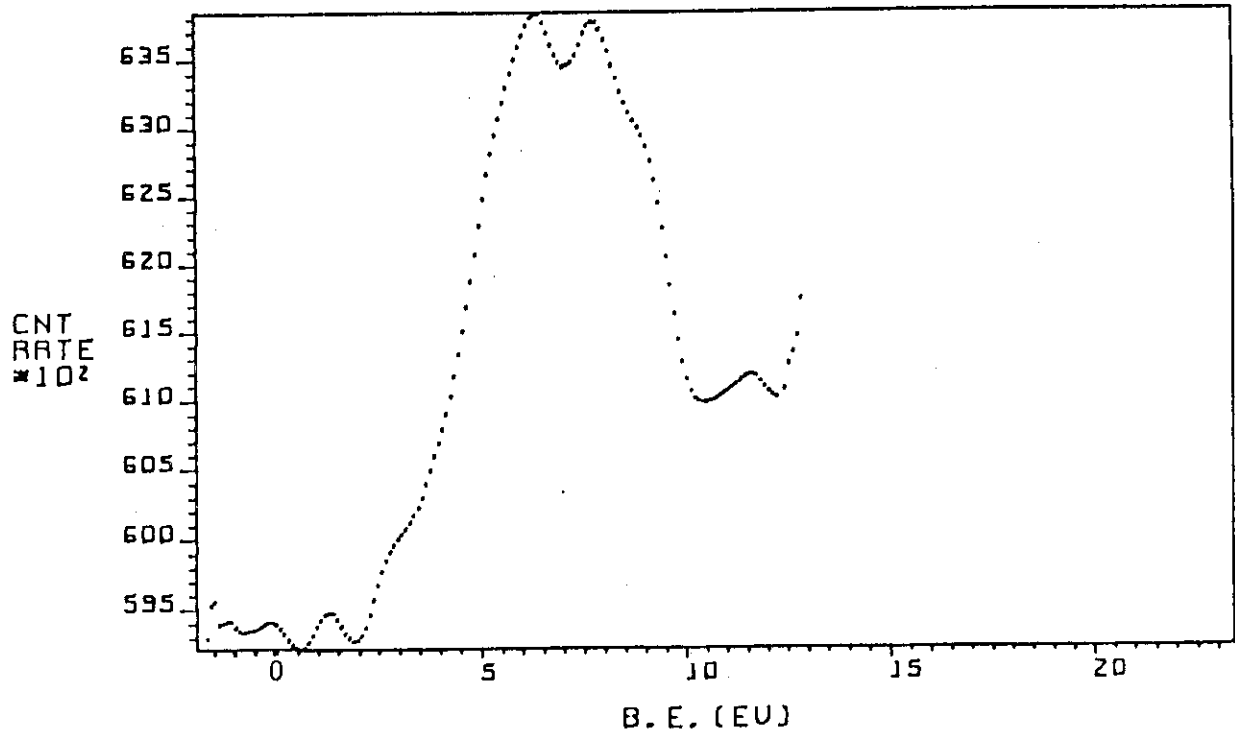


Fig. 26 Valence-band spectrum of ZrO₂.

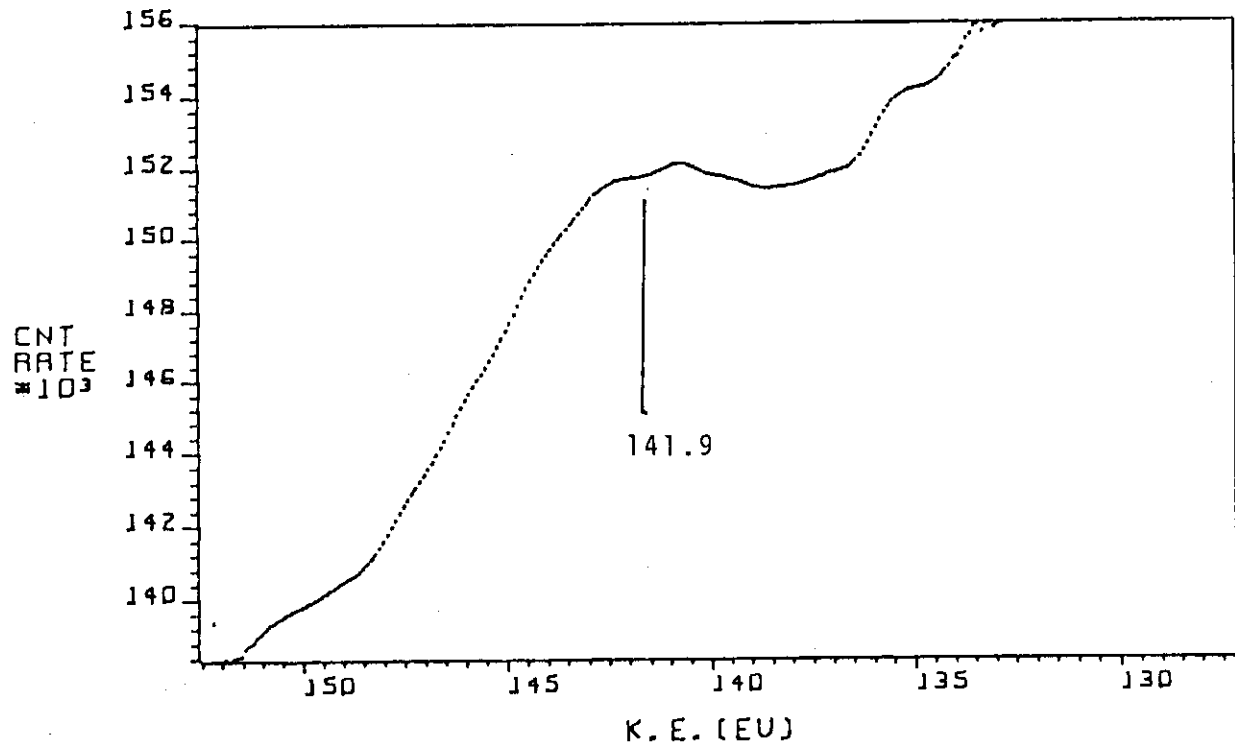


Fig. 27 M_{4,5} N_{2,3} V XAES spectrum of ZrO₂.

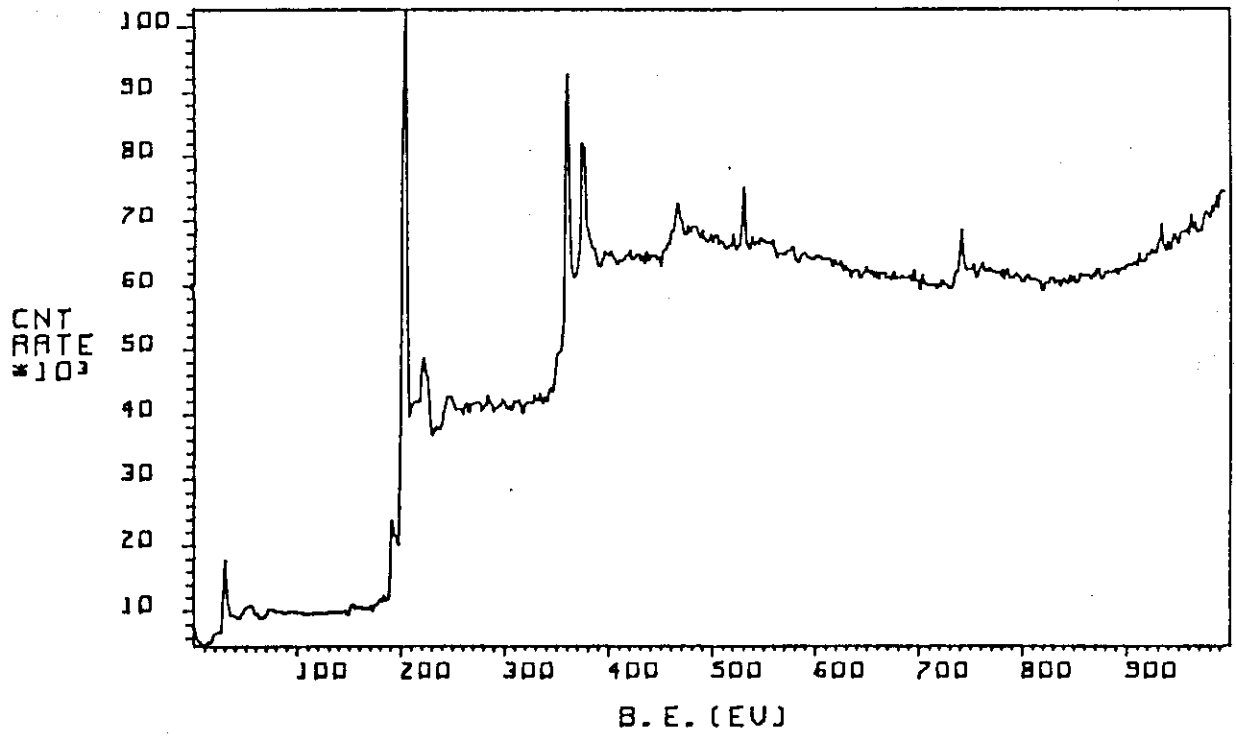


Fig. 28 XPS wide scan of Nb_{fl}.

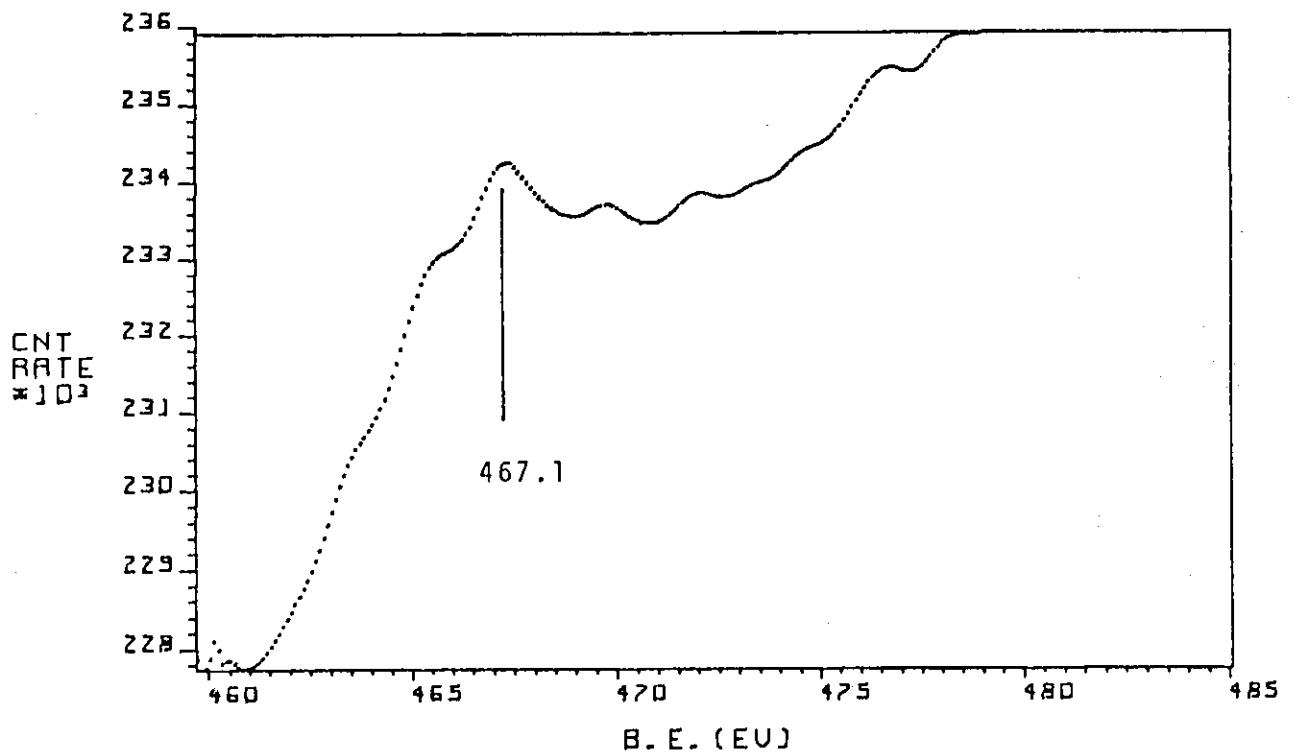


Fig. 29 Nb_{3s} XPS spectrum of Nb_{fl}.

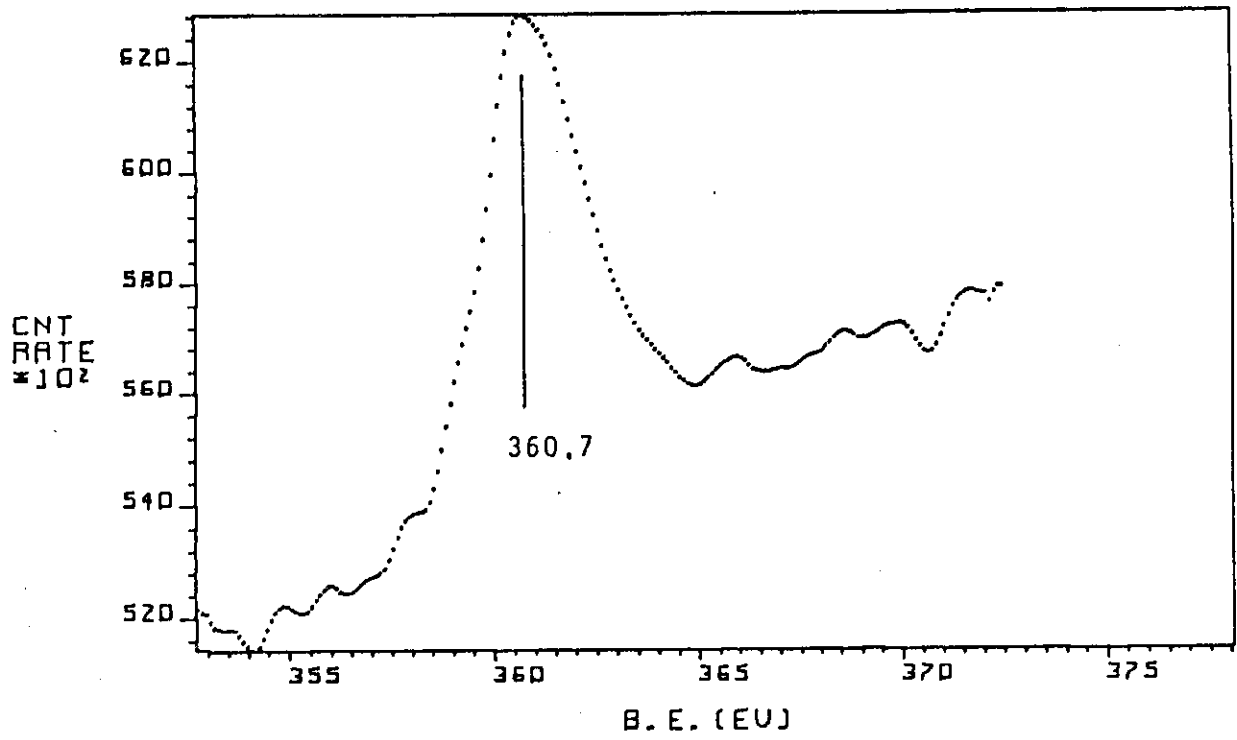


Fig. 30 Nb3p XPS spectrum of Nb_{fl}.

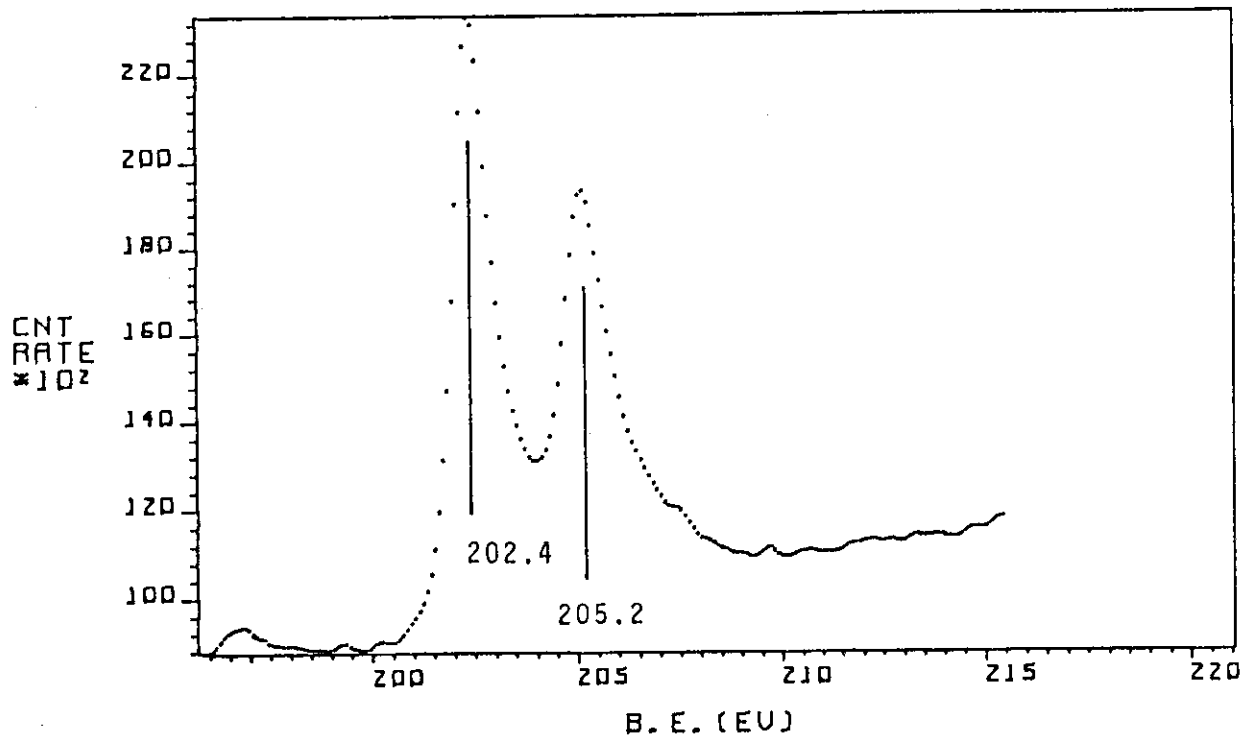


Fig. 31 Nb3d XPS spectrum of Nb_{fl}.

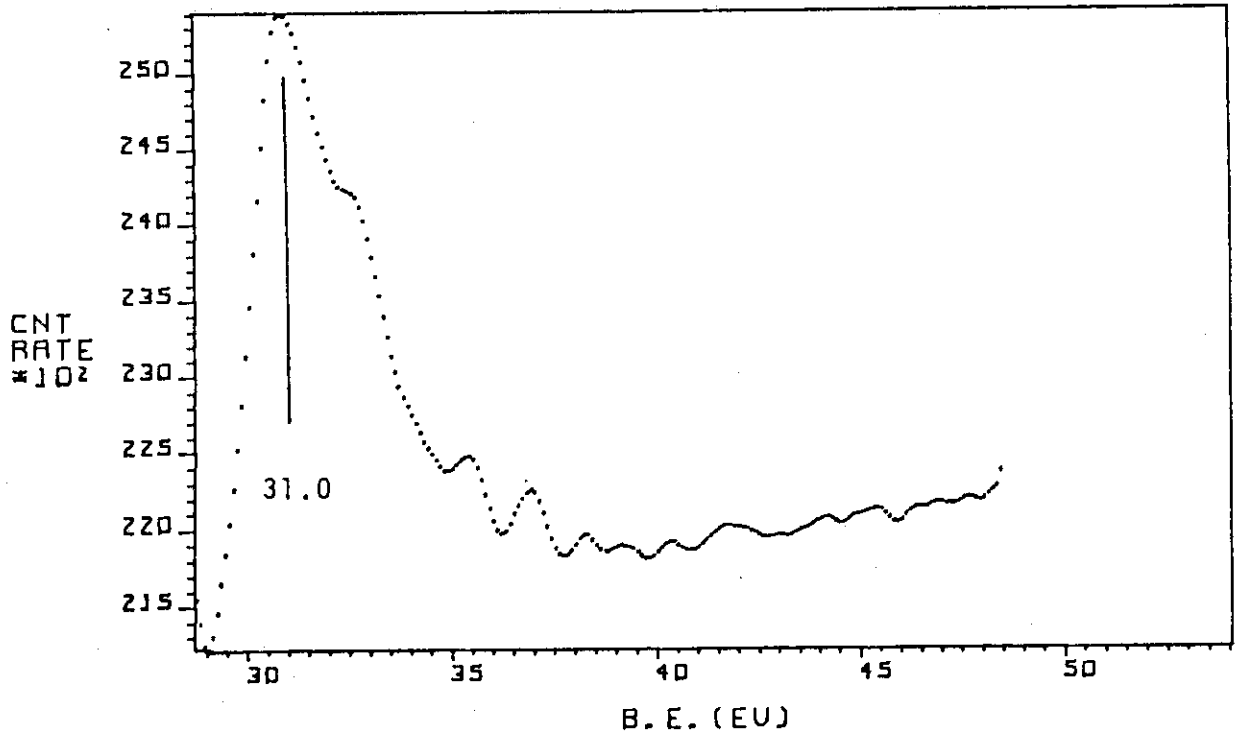


Fig. 32 Nb_{4p} XPS spectrum of Nb_{fl}.

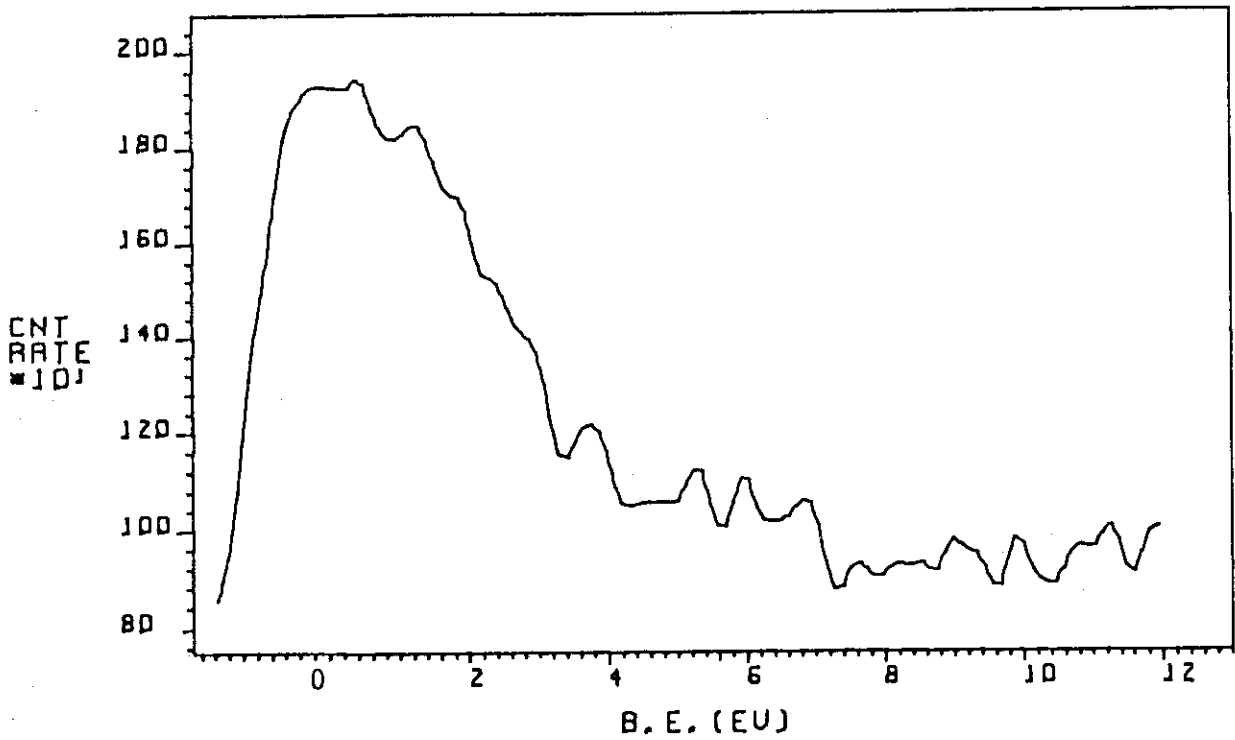


Fig. 33 Valence-band spectrum of Nb_{fl}.

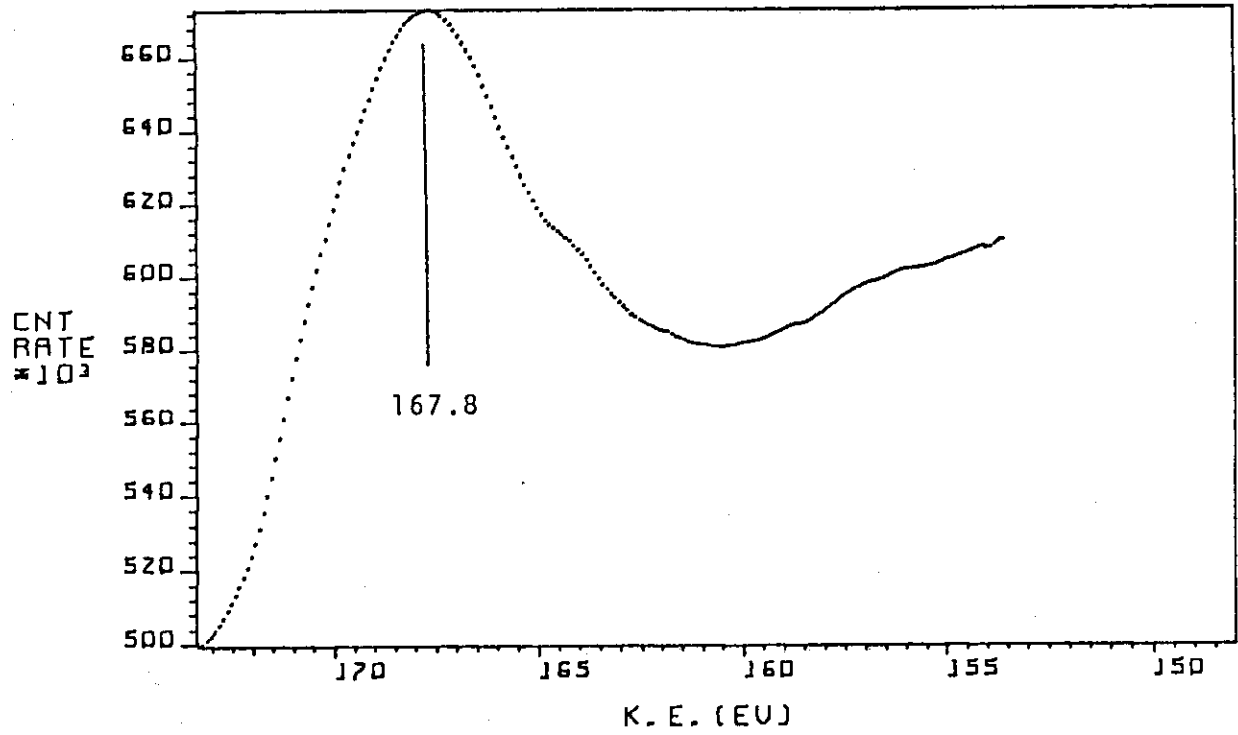


Fig. 34 $M_{4,5}N_{2,3}V$ XAES spectrum of Nb_{fz}.

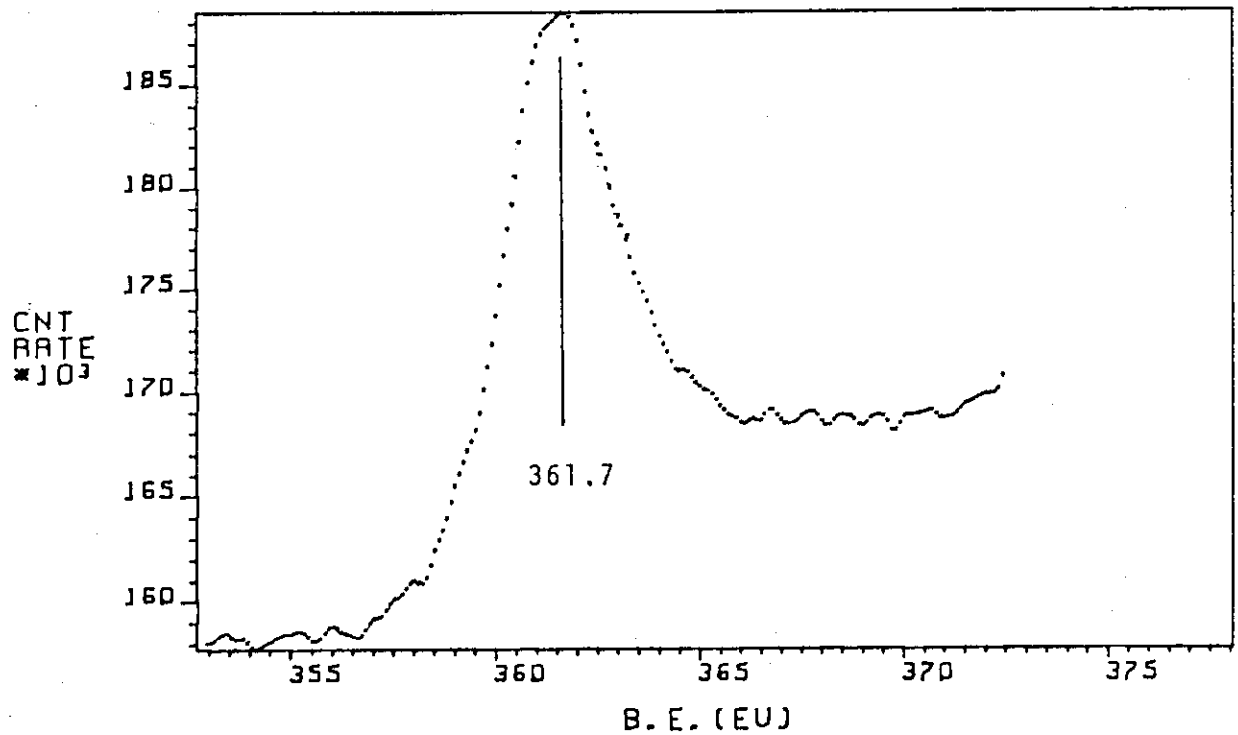


Fig. 35 Nb3p XPS spectrum of Nb_{et}.

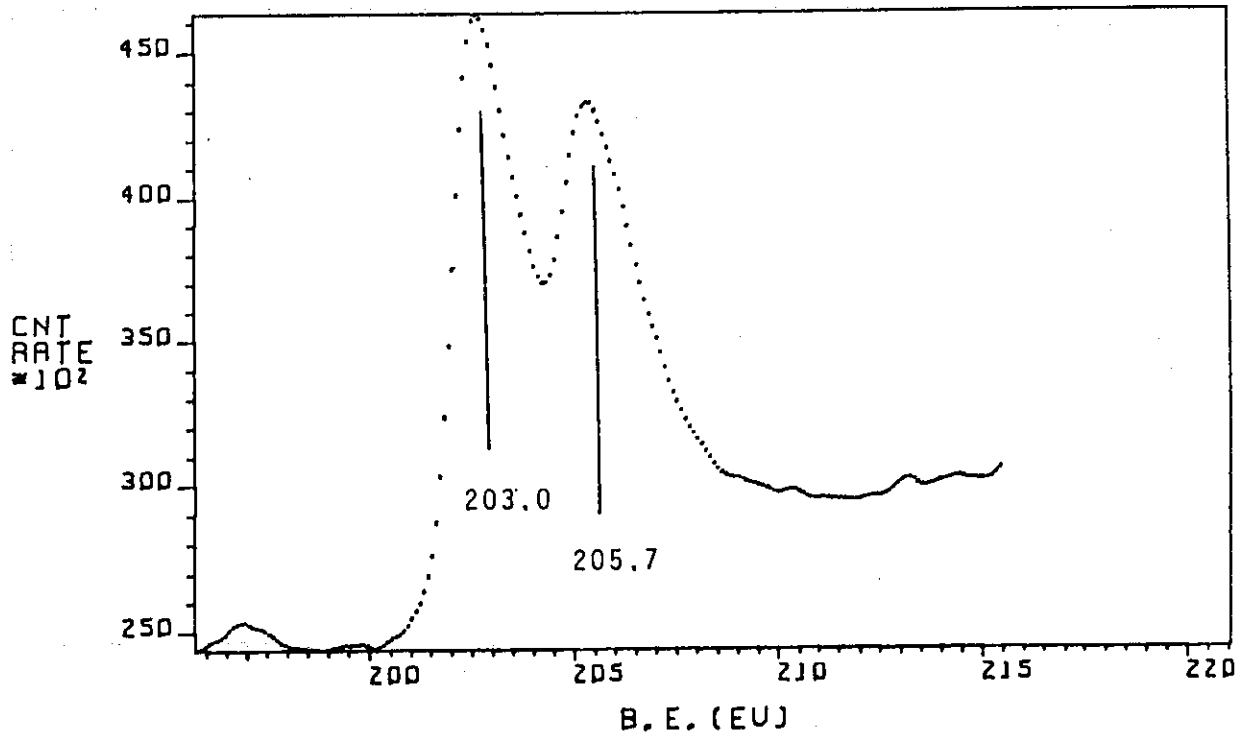


Fig. 36 Nb_{3d} XPS spectrum of Nb_{et}.

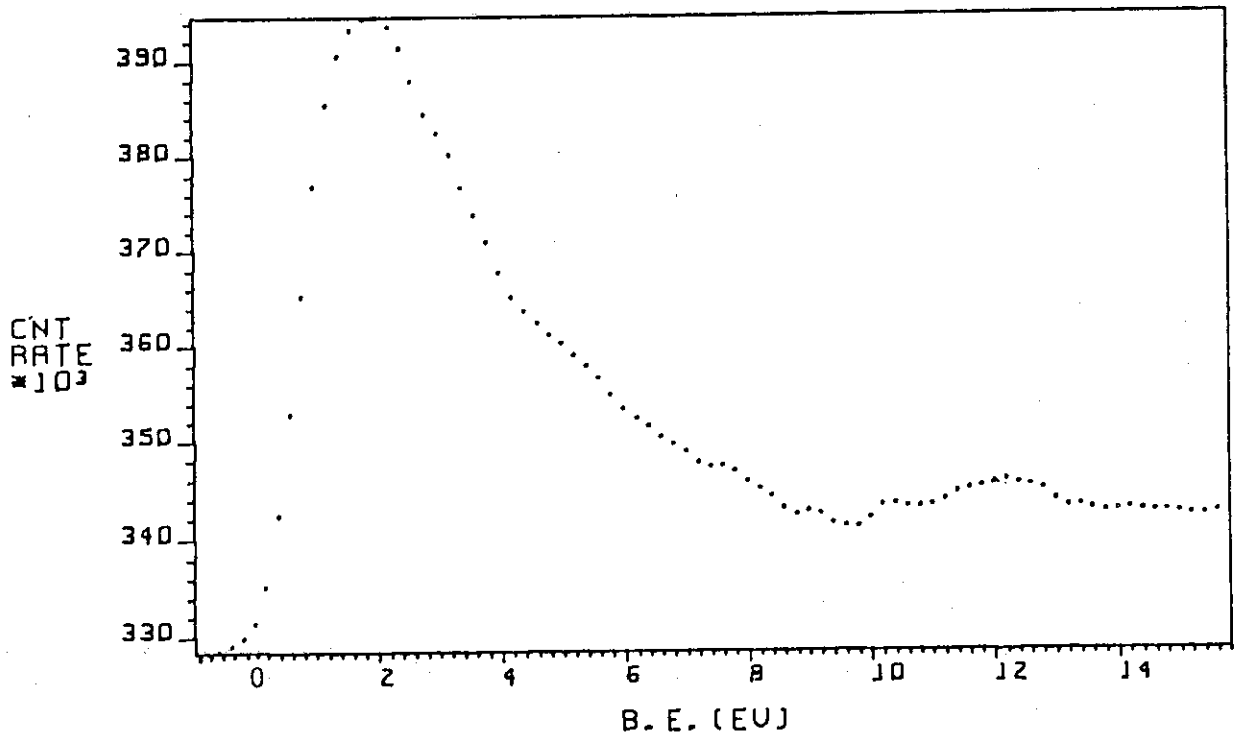


Fig. 37 Valence-band spectrum of Nb_{et}.

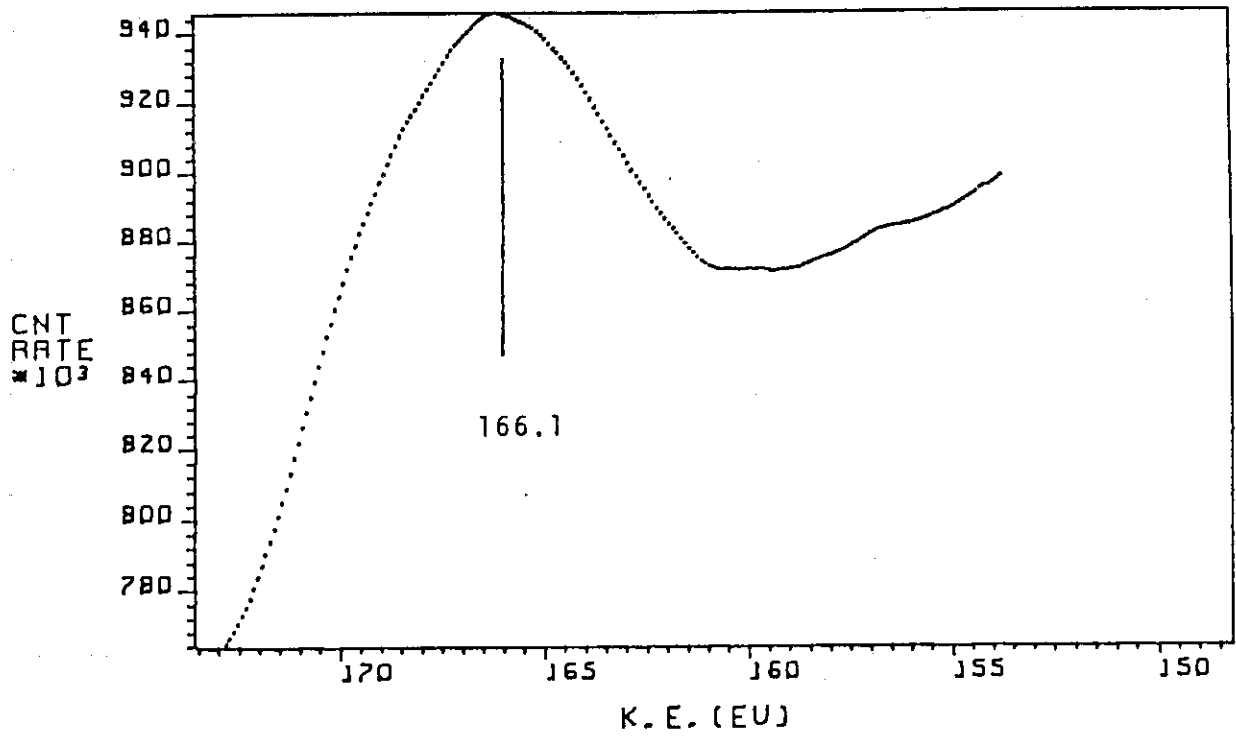


Fig. 38 M_{4,5}N_{2,3}V XAES spectrum of Nb_{et}.

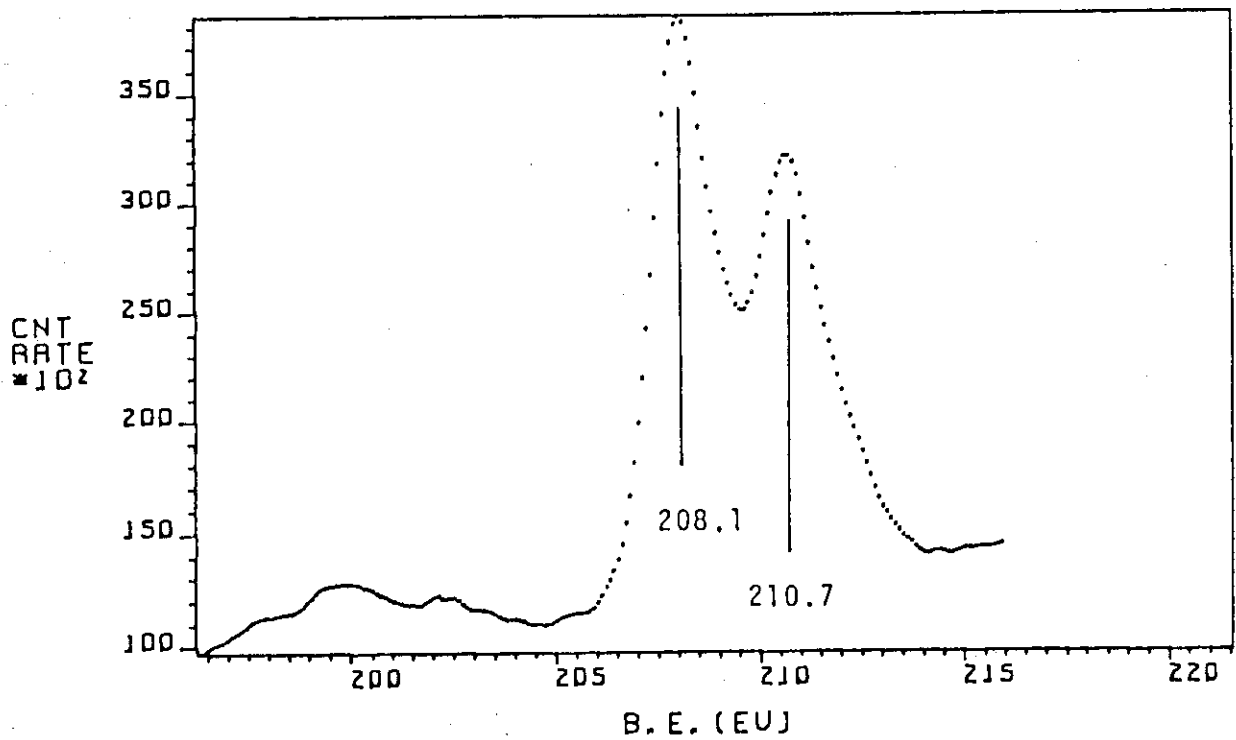


Fig. 39 Nb_{3d} XPS spectrum of Nb₂O₅.

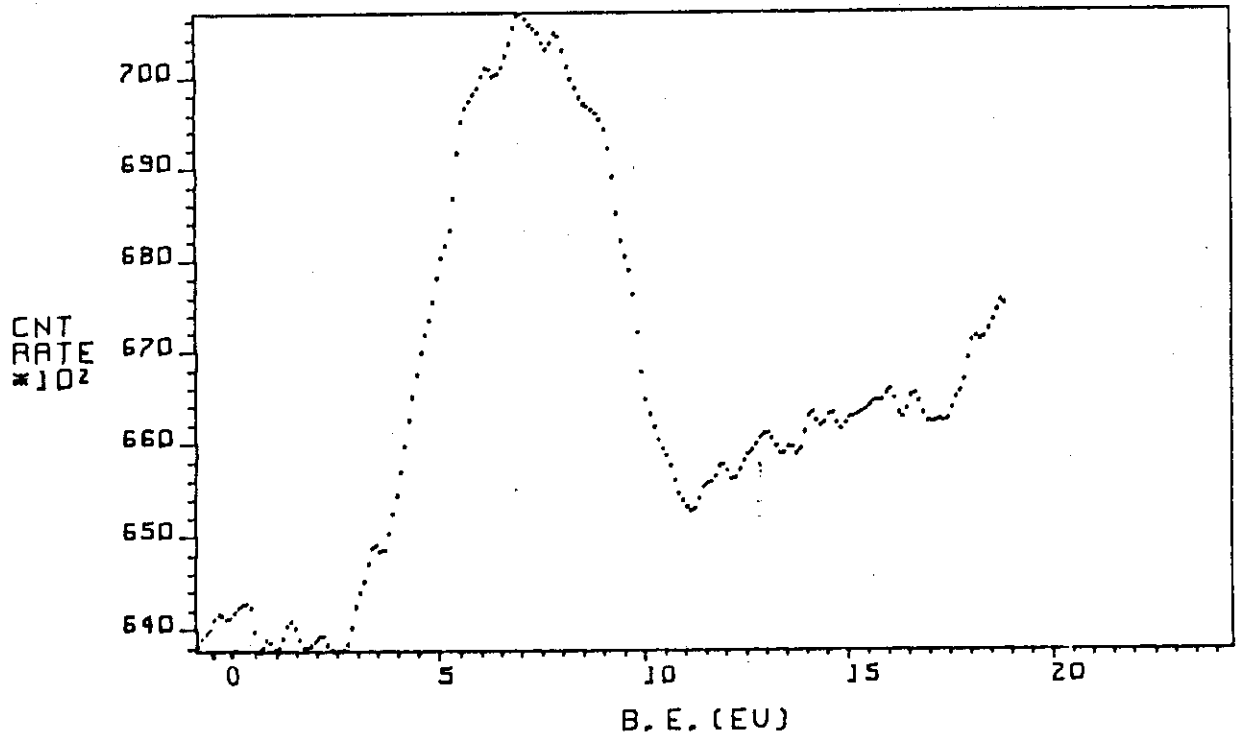


Fig. 40 Valence-band spectrum of Nb₂O₅.

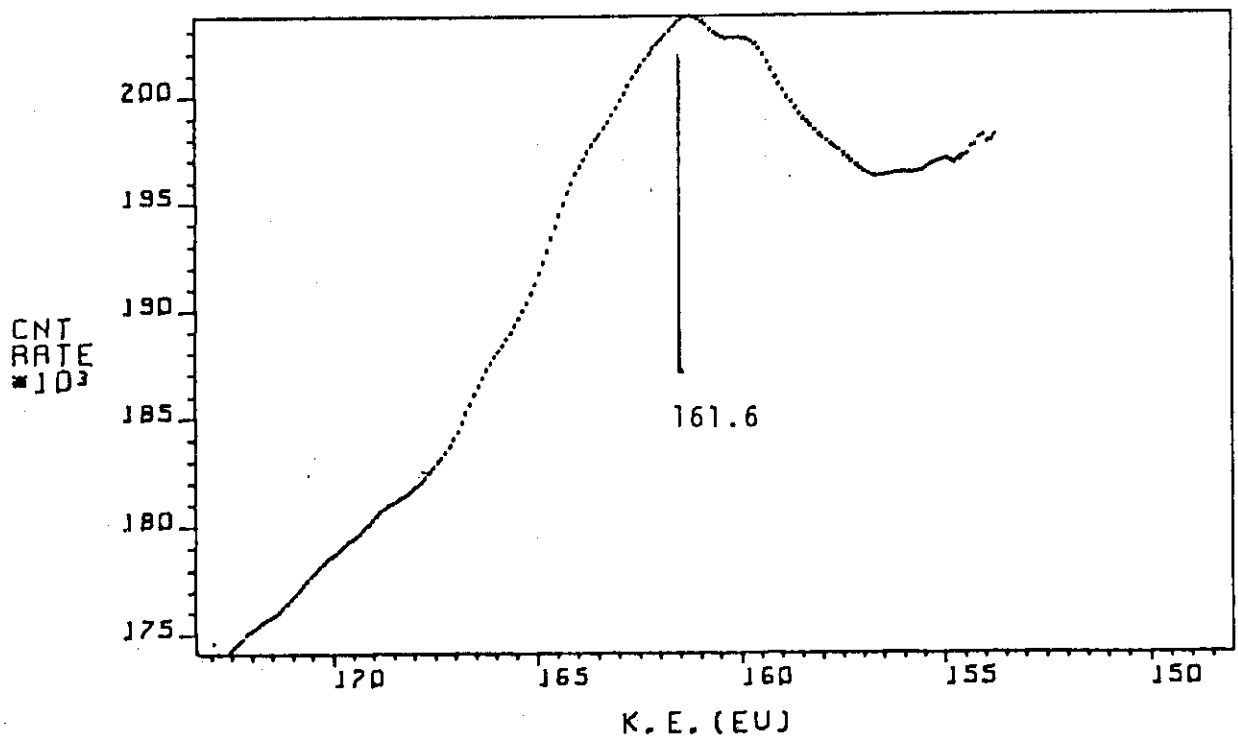


Fig. 41 M_{4,5}N_{2,3}V XAES spectrum of Nb₂O₅.

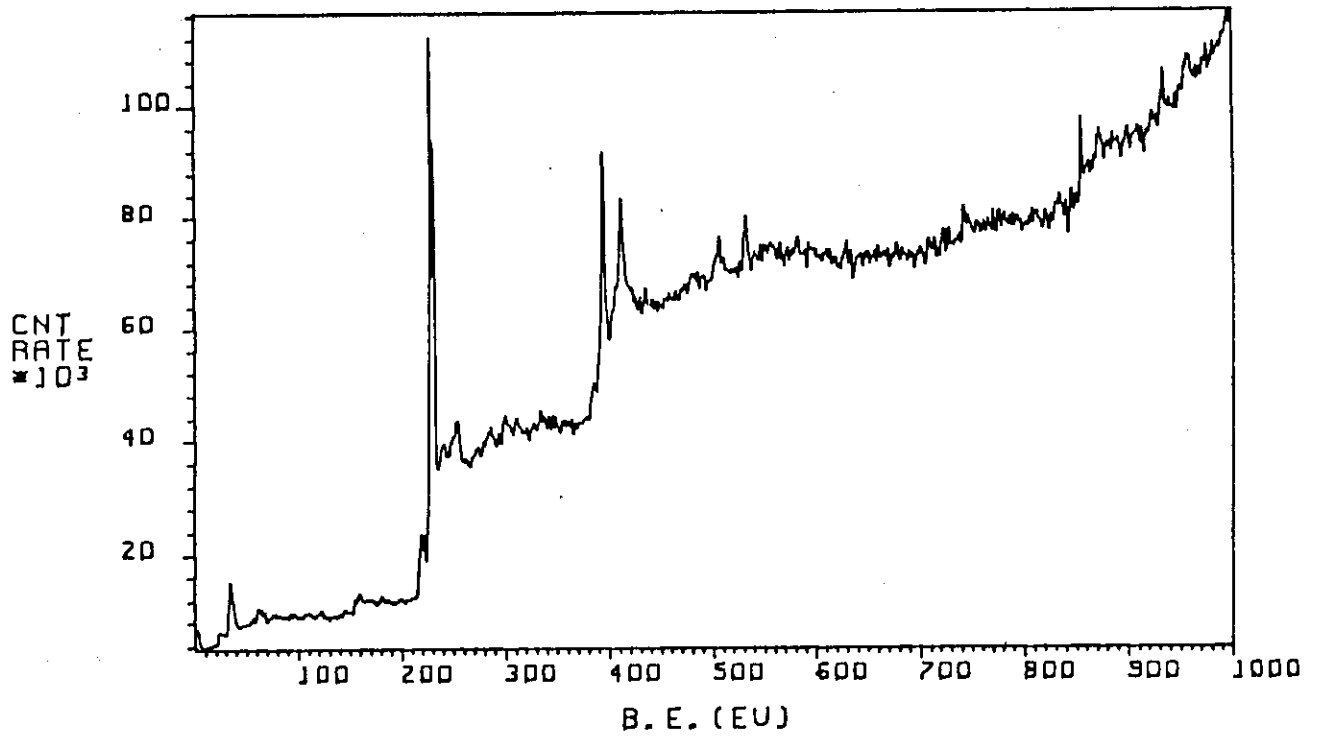


Fig. 42 XPS wide scan of Mo_{fl}.

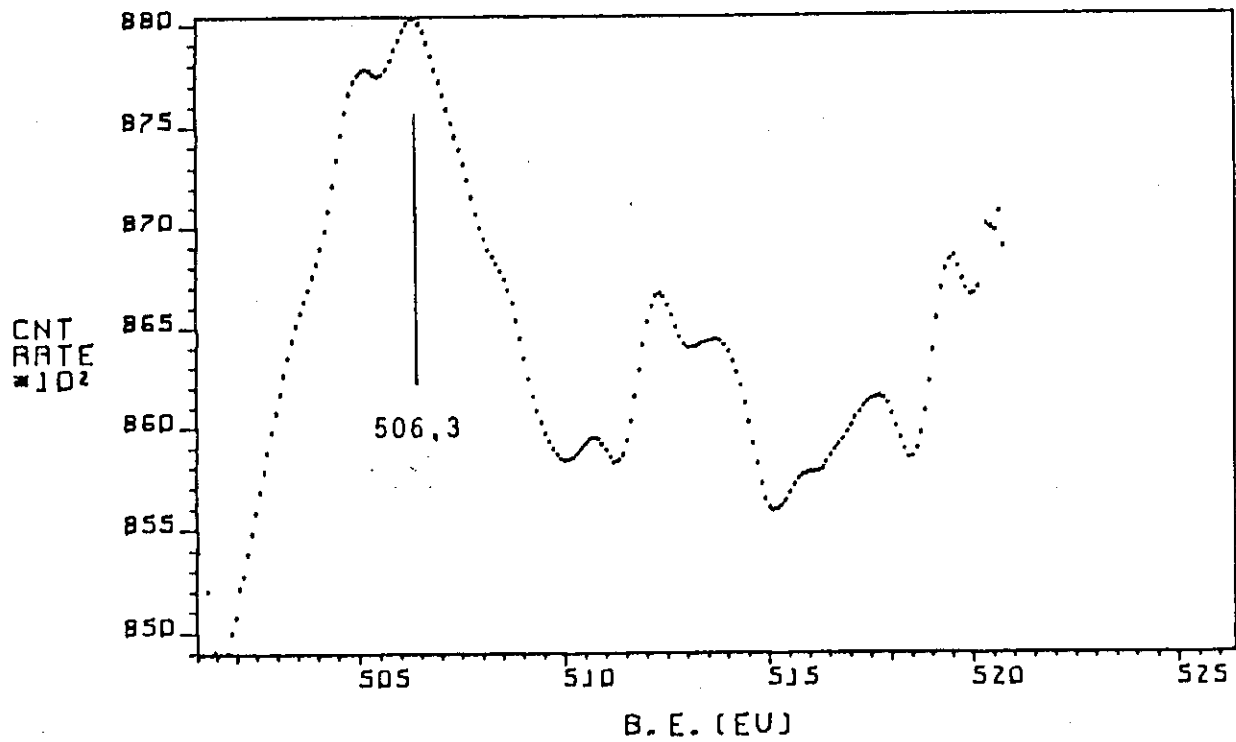


Fig. 43 Mo_{3s} XPS spectrum of Mo_{fl}.

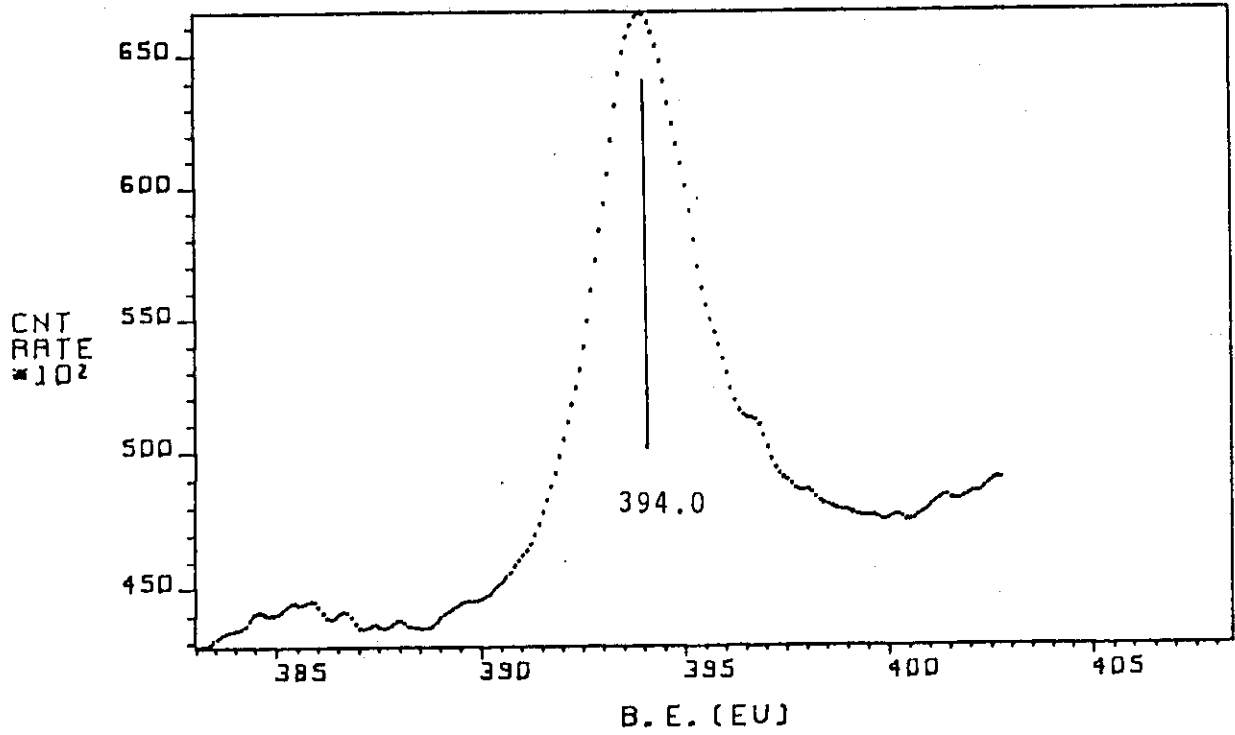


Fig. 44 Mo3p XPS spectrum of Mo_{fl}.

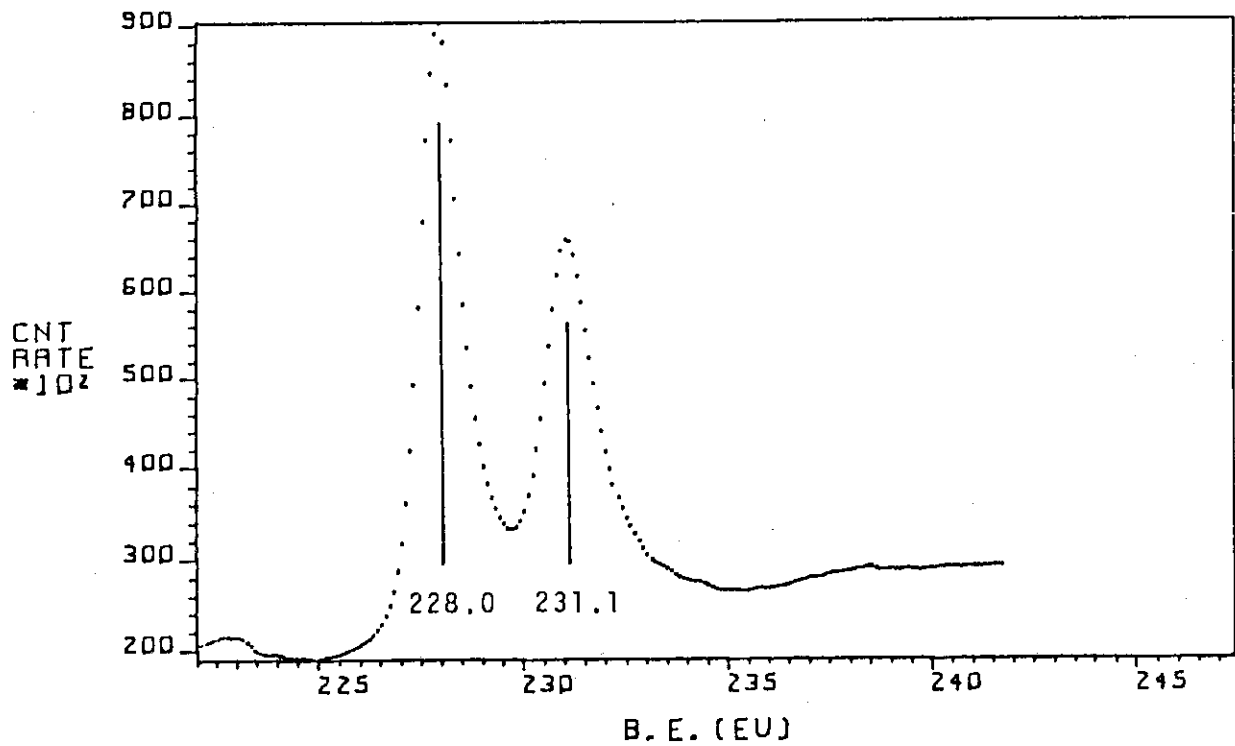


Fig. 45 Mo3d XPS spectrum of Mo_{fl}.

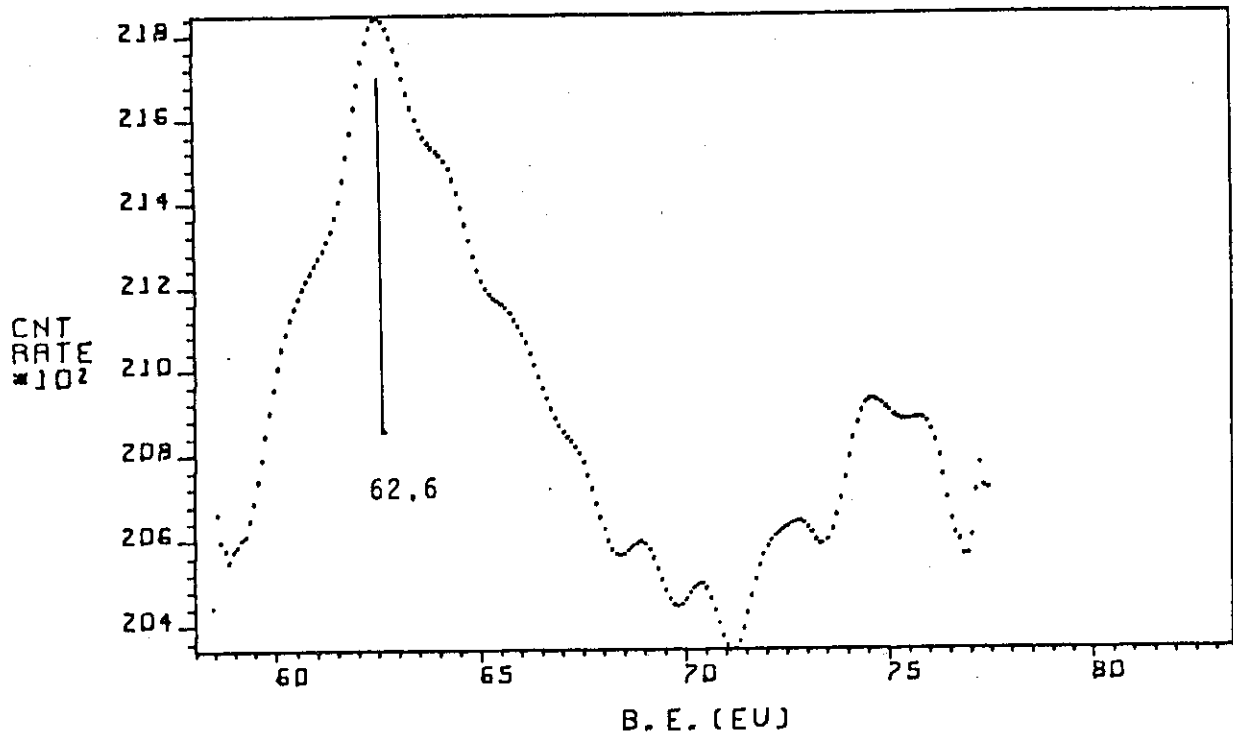


Fig. 46 Mo_{4s} XPS spectrum of Mo_{fz}.

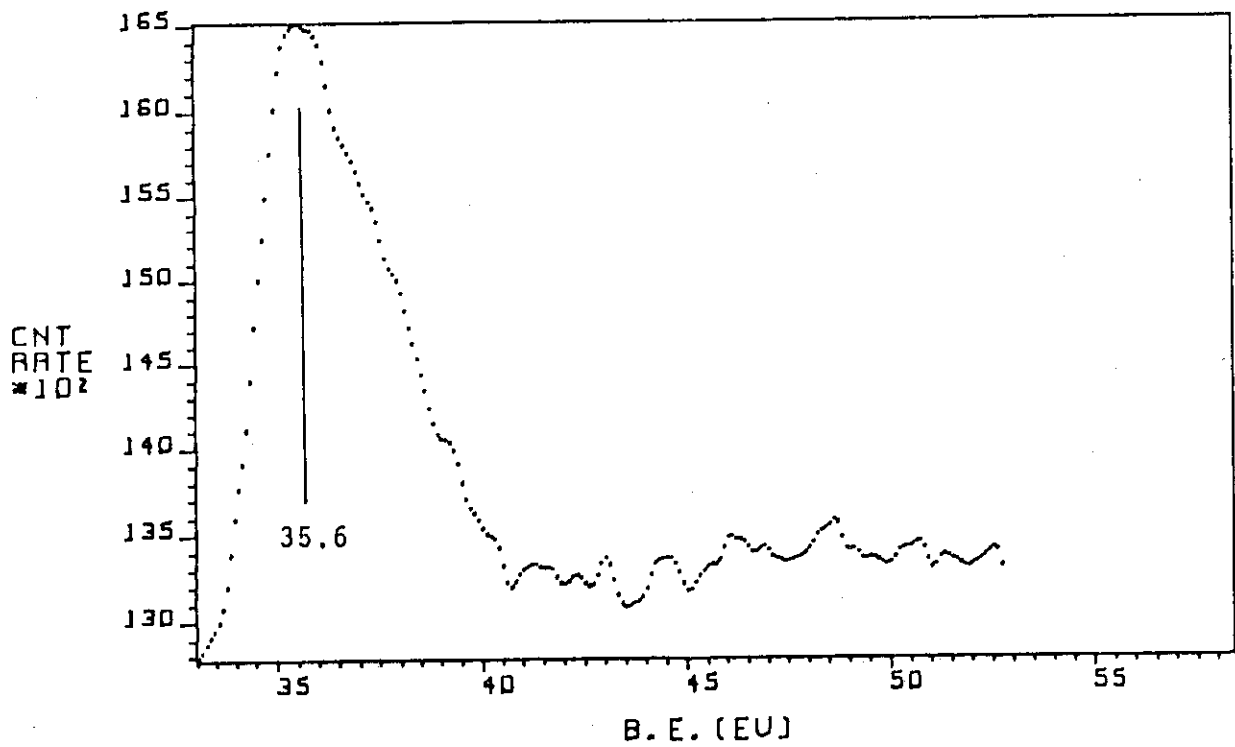


Fig. 47 Mo_{4p} XPS spectrum of Mo_{fz}.

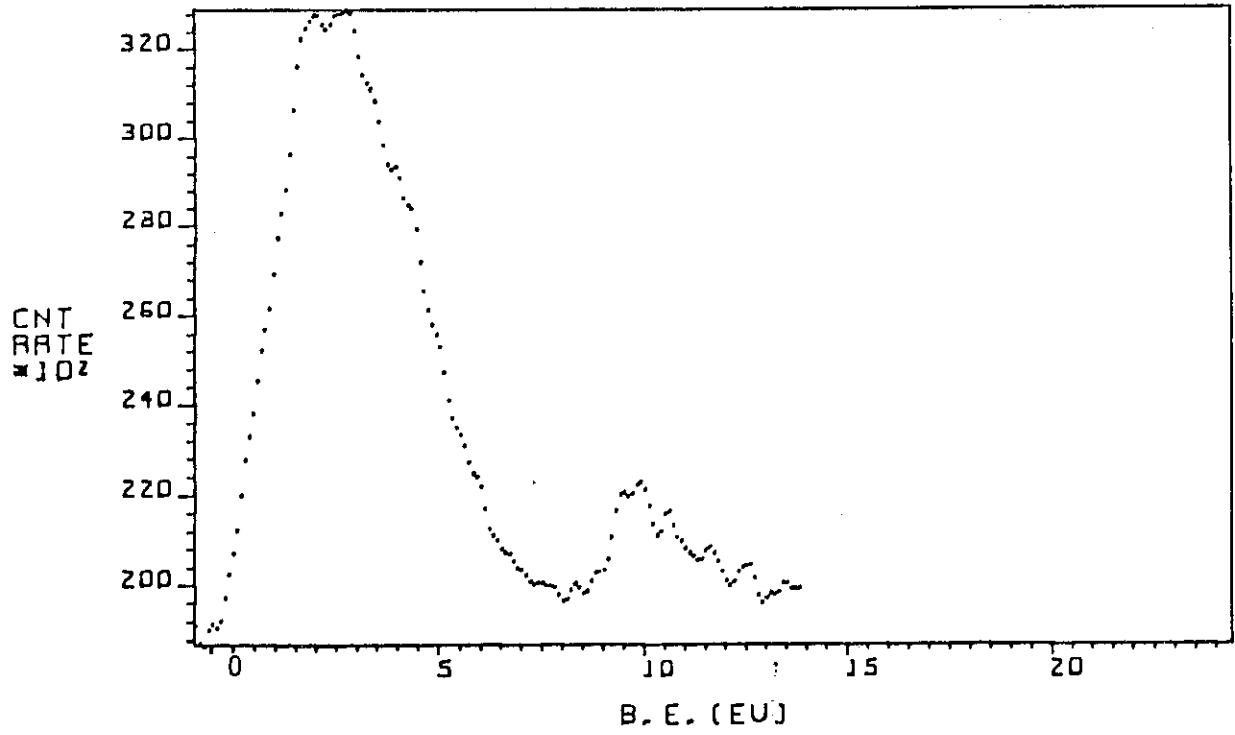


Fig. 48 Valence-band spectrum of Mo_{fl}.

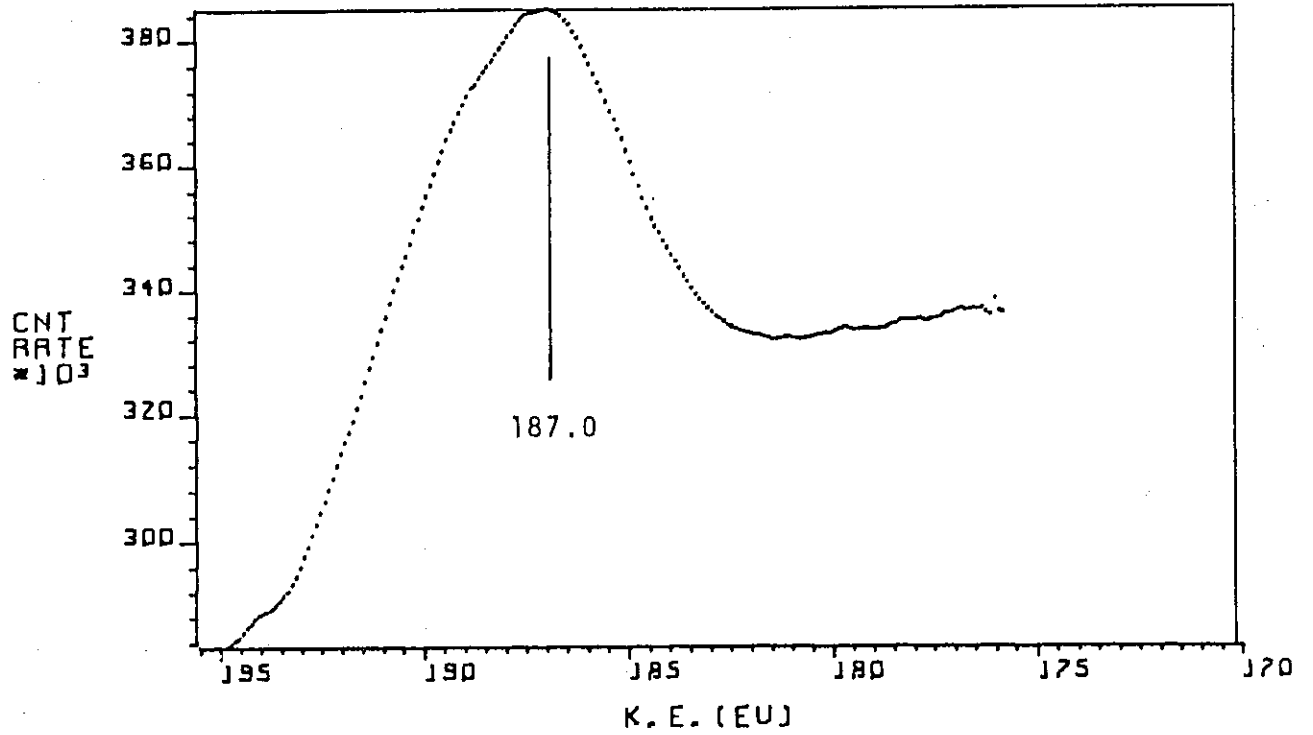


Fig. 49 M_{4,5}N_{2,3}V XAES spectrum of Mo_{fl}.

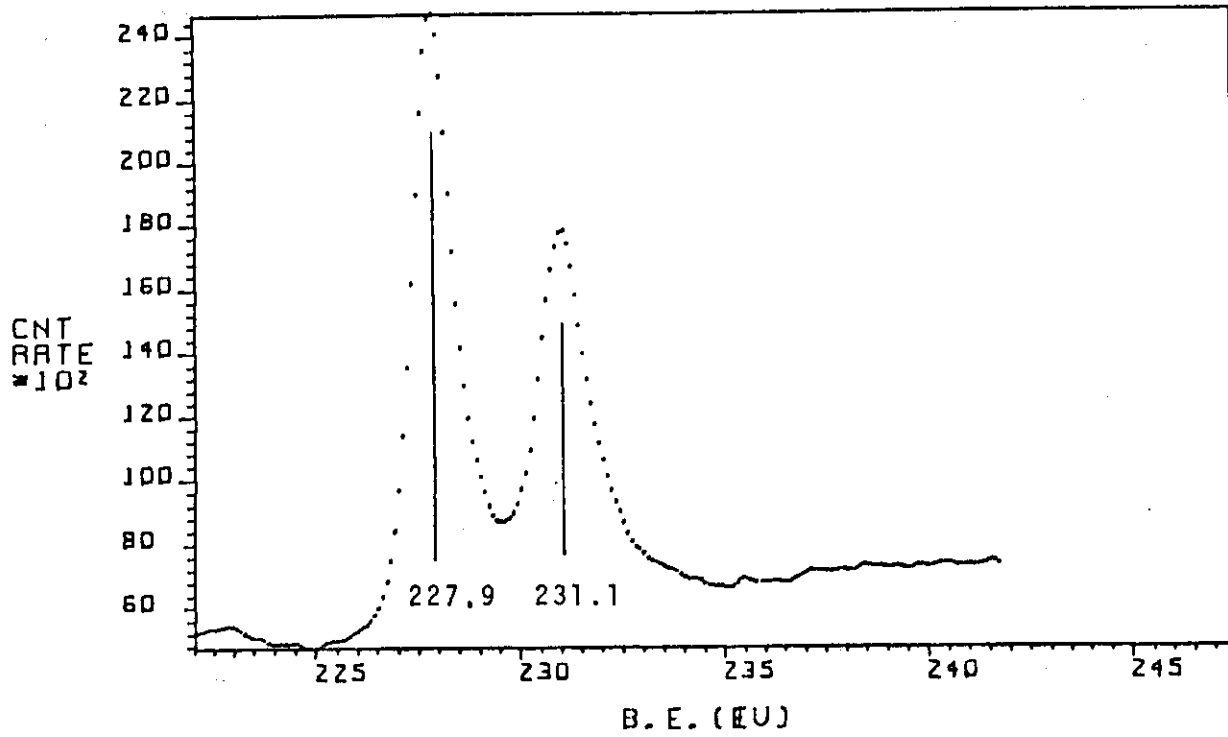


Fig. 50 Mo_{3d} XPS spectrum of Mo_{et}.

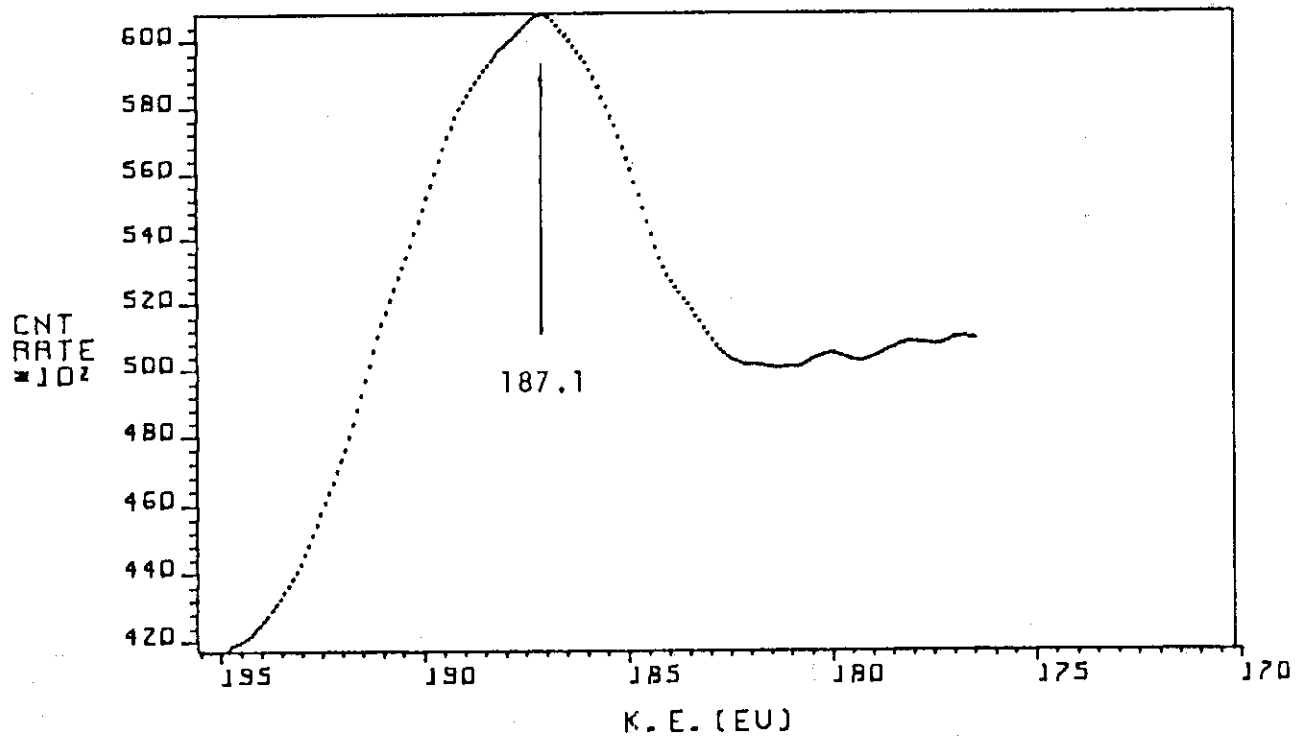


Fig. 51 M_{4,5}N_{2,3}V XAES spectrum of Mo_{et}.

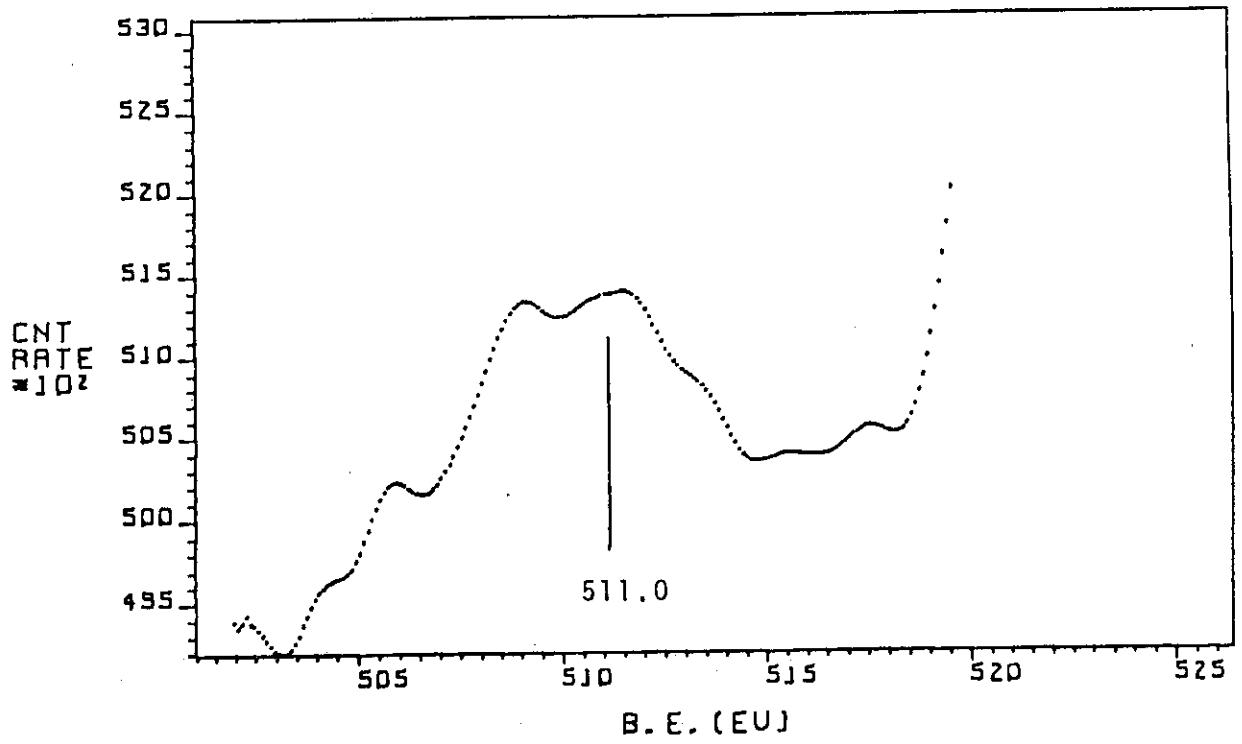


Fig. 52 Mo_{3s} XPS spectrum of MoO₃.

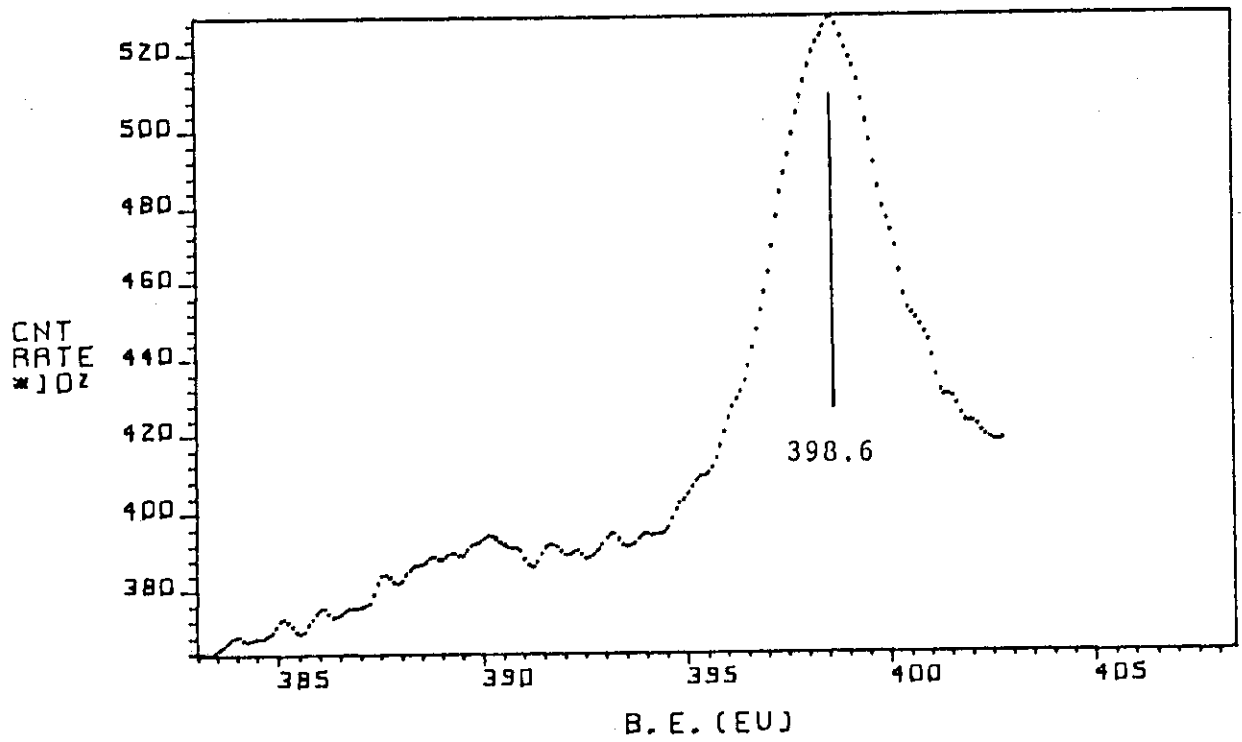


Fig. 53 Mo_{3p} XPS spectrum of MoO₃.

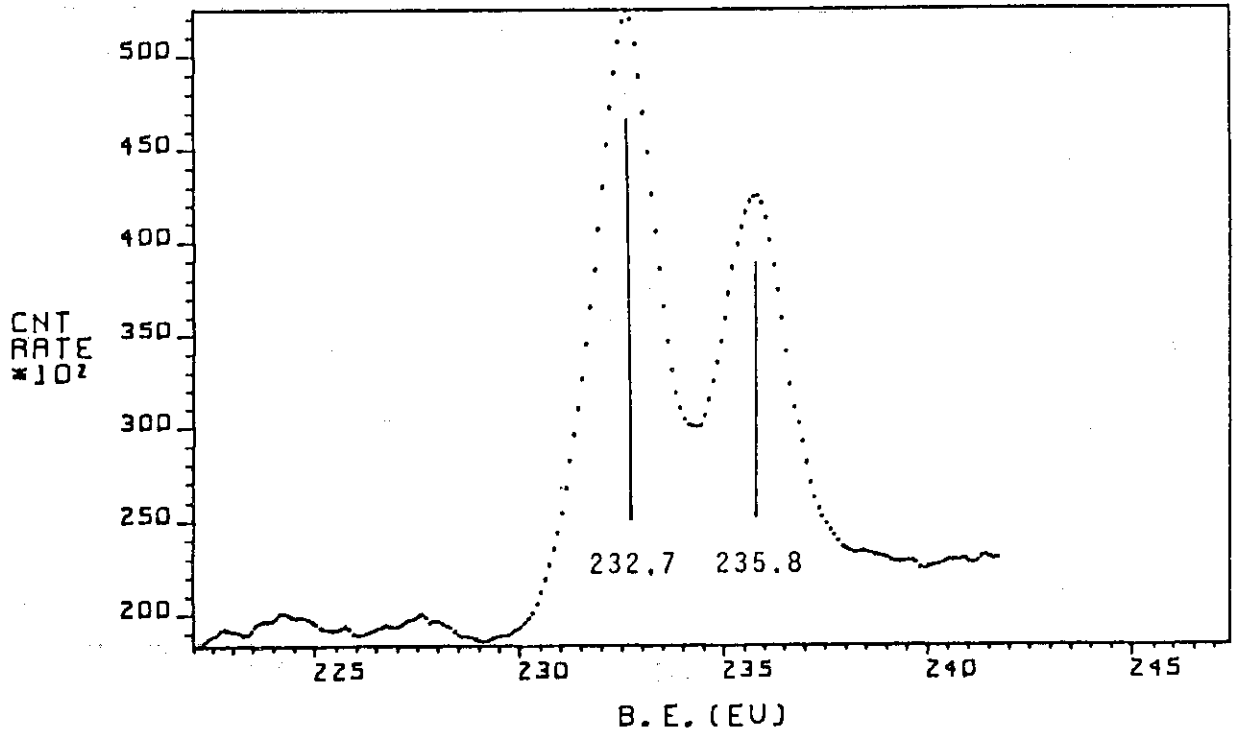


Fig. 54 Mo3d XPS spectrum of MoO₃.

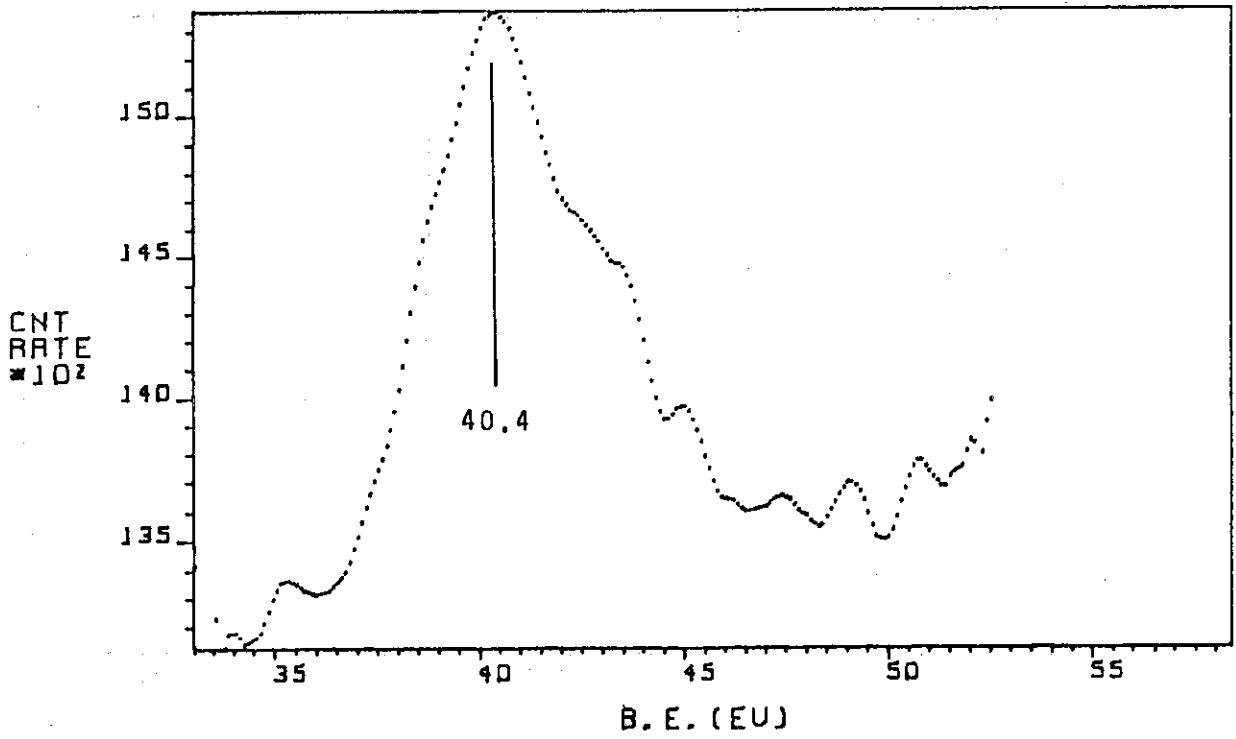


Fig. 55 Mo4p XPS spectrum of MoO₃.

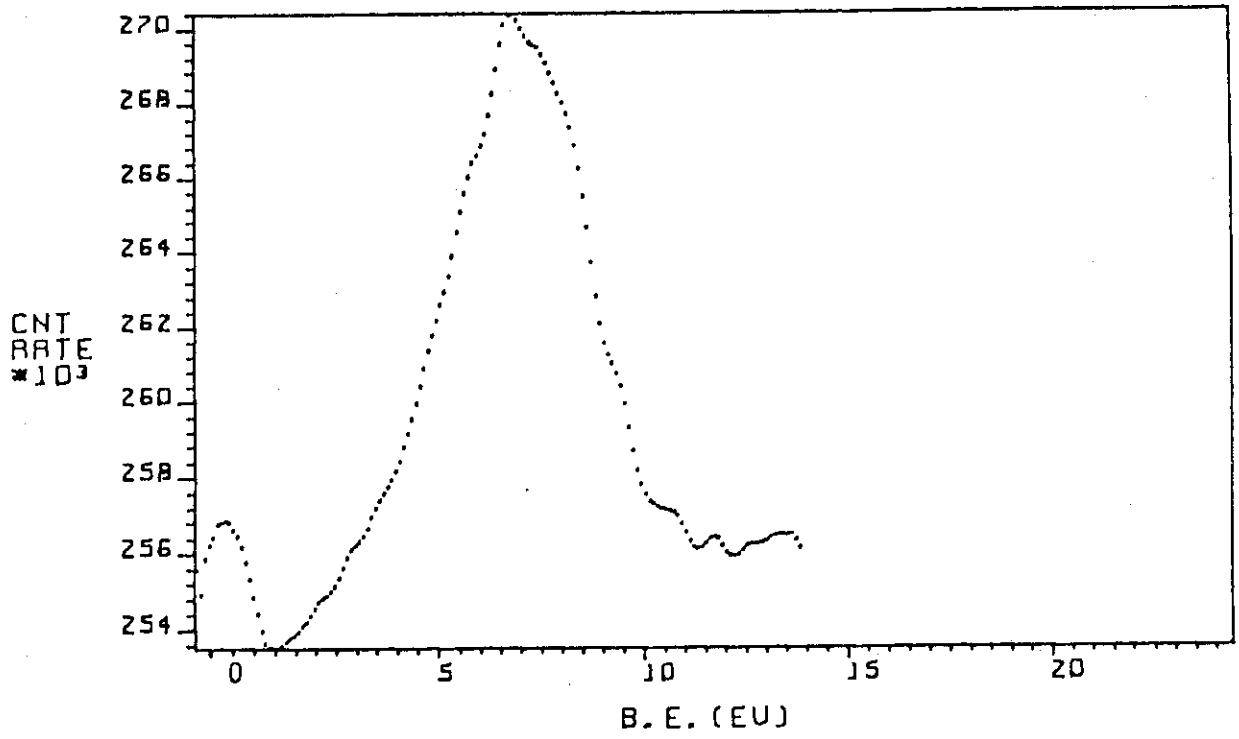


Fig. 56 Valence-band spectrum of MoO₃.

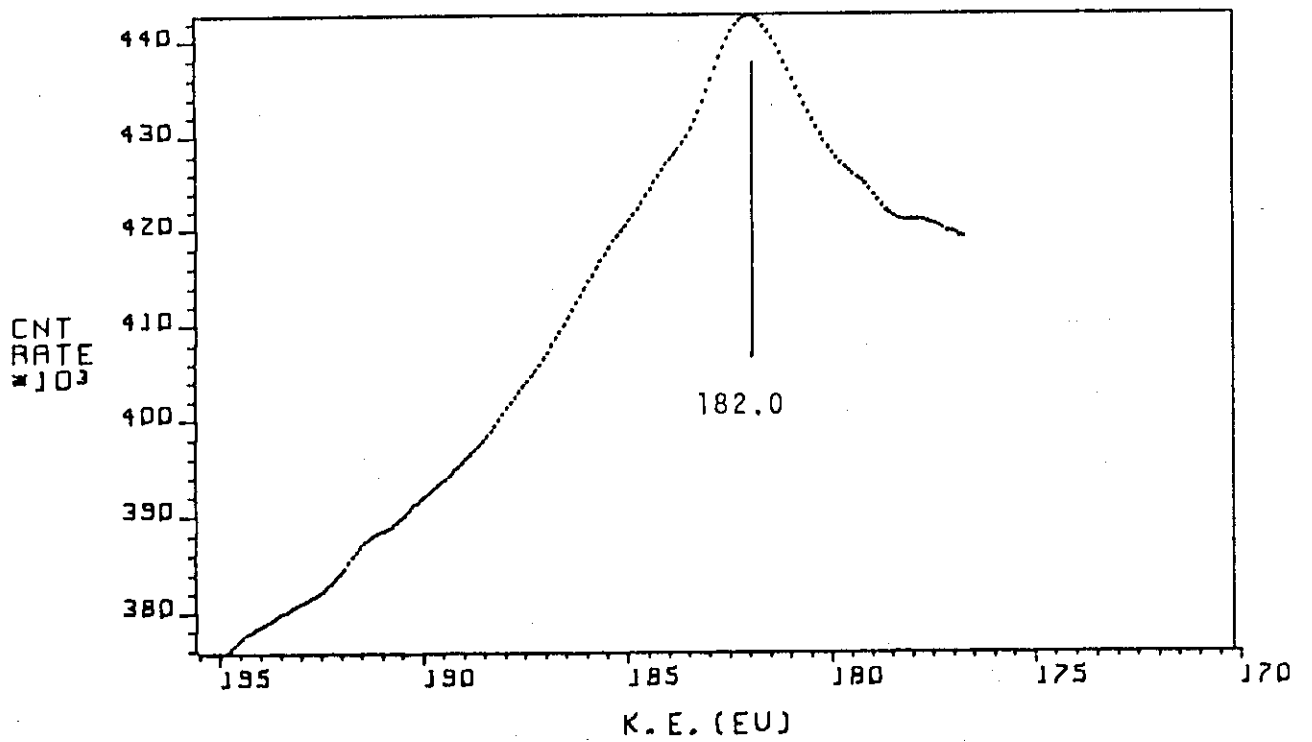


Fig. 57 M_{4,5}N_{2,3}V XAES spectrum of MoO₃.

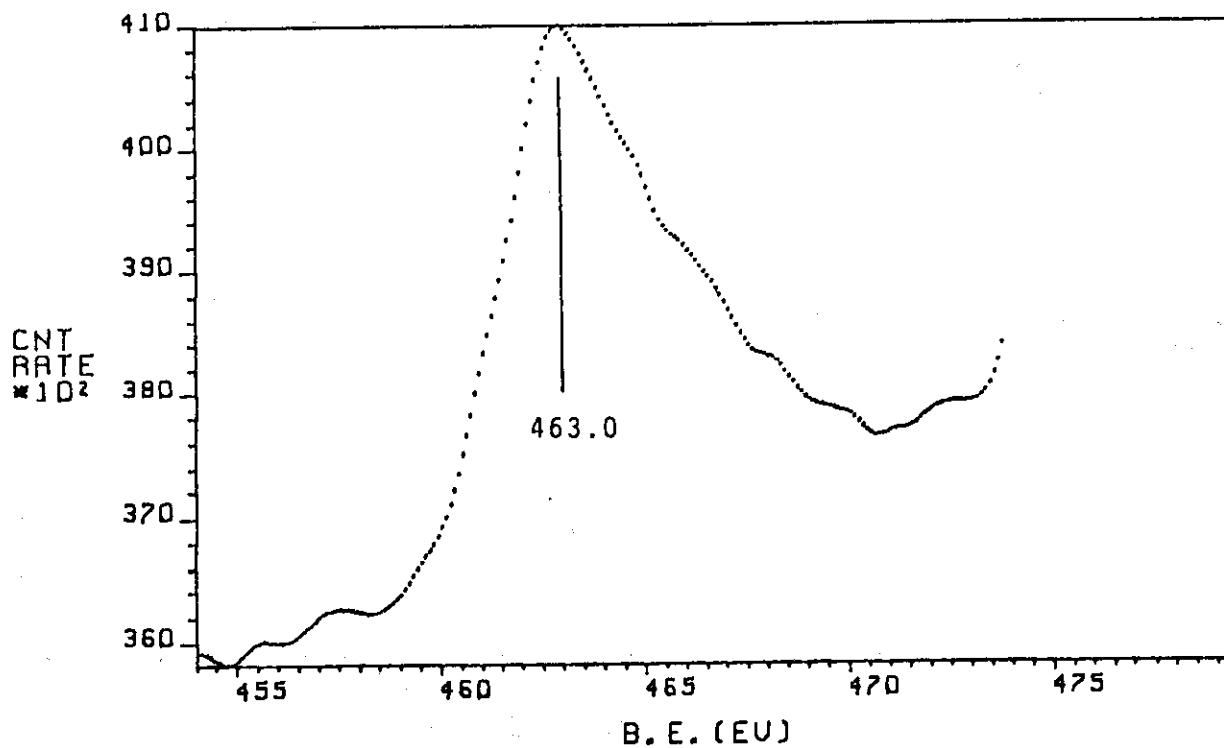


Fig. 58 Ru3p XPS spectrum of RuO₂.

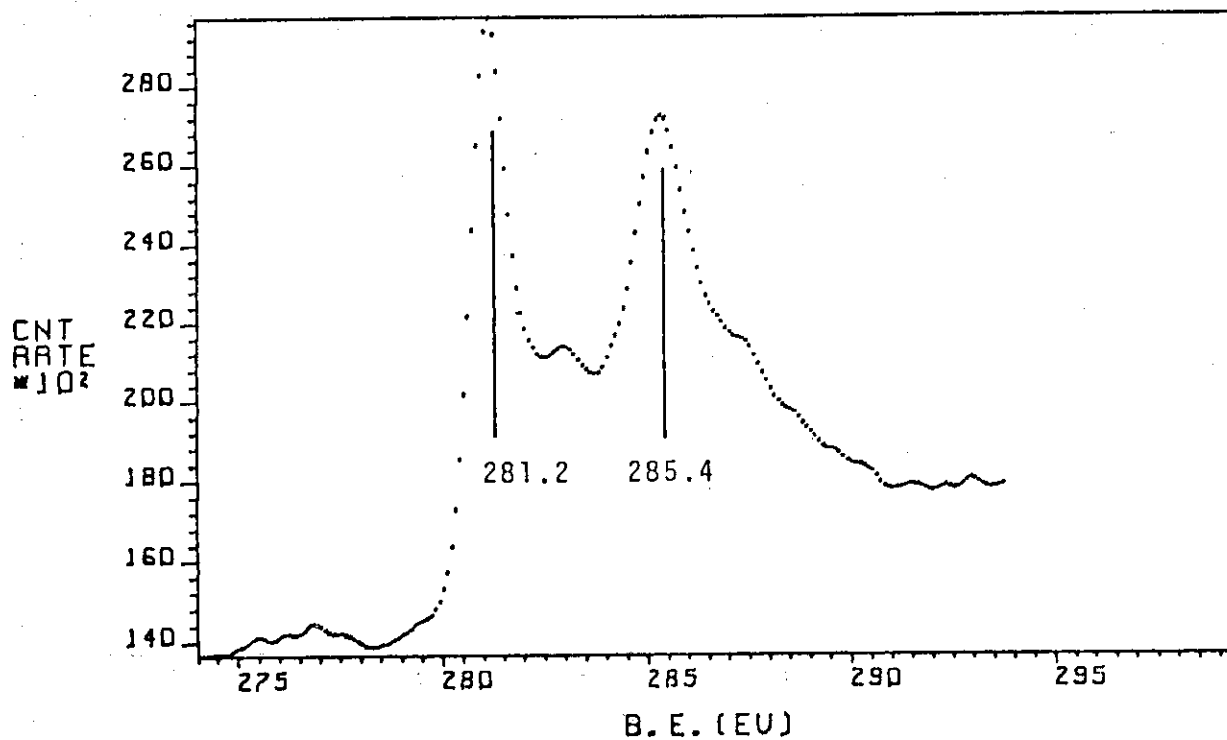


Fig. 59 Ru3d XPS spectrum of RuO₂.

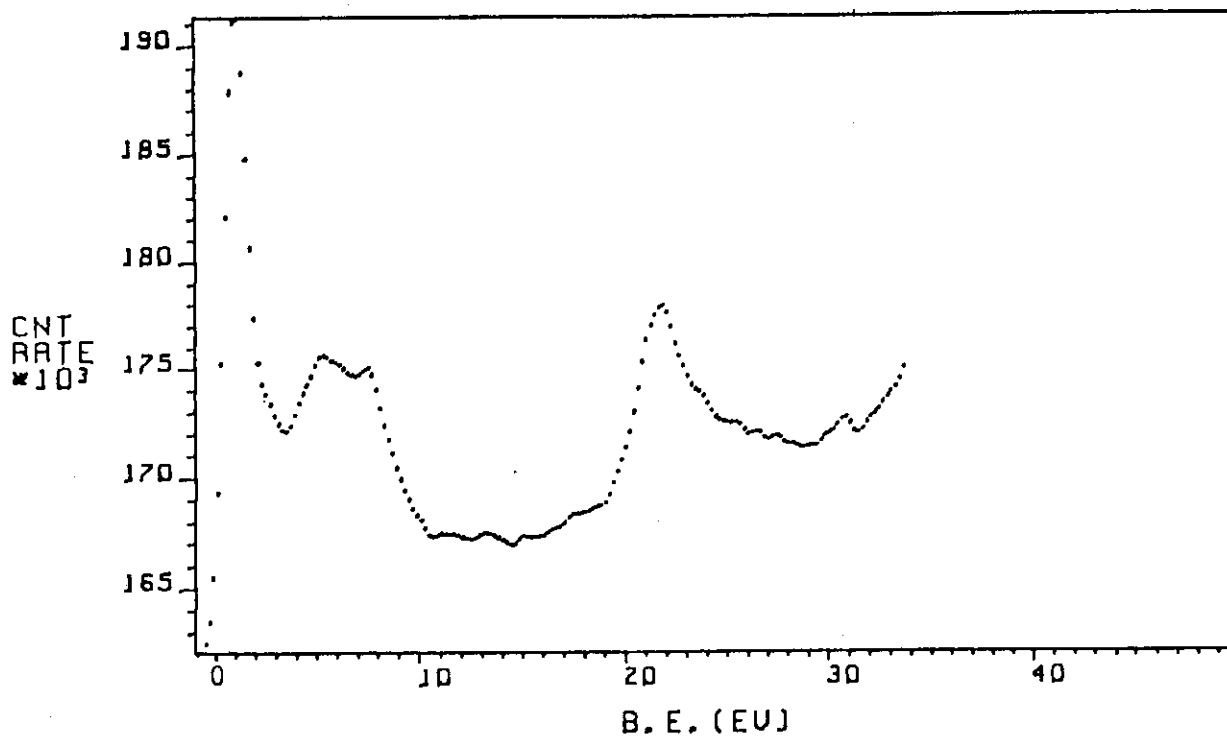


Fig. 60 Valence-band spectrum of RuO₂.